J. Plasma Phys. (2021), *vol*. 87, 905870202
Published by Cambridge University Press
doi:10.1017/S0022377821000027

Effect of external magnetic field on lane formation in driven pair-ion plasmas

Swati Baruah [1],†, **U. Sarma**[1] **and R. Ganesh** [2]

[1]Kaziranga University, Jorhat, Assam 785006, India

[2]Institute for Plasma Research, Bhat, Gandhinagar, Gujarat 382428, India

(Received 9 October 2020; revised 8 January 2021; accepted 8 January 2021)

Lane formation dynamics in externally driven pair-ion plasma (PIP) particles is studied in the presence of external magnetic field using Langevin dynamics (LD) simulation. The phase diagram obtained distinguishing the no-lane and lane states is systematically determined from a study of various Coulomb coupling parameter values. A peculiar lane formation-disintegration parameter space is identified; lane formation area extended to a wide range of Coulomb coupling parameter values is observed before disappearing to a mixed phase. The different phases are identified by calculating the order parameter. This and the critical parameters are calculated directly from LD simulation. The critical electric field strength value above which the lanes are formed distinctly is obtained, and it is observed that in the presence of the external magnetic field, the PIP system requires a higher value of the electric field strength to enter into the lane formation state than that in the absence of the magnetic field. We further find out the critical value of electric field frequency beyond which the system exhibits a transition back to the disordered state and this critical frequency is found as an increasing function of the electric field strength in the presence of an external magnetic field. The movement of the lanes is also observed in a direction perpendicular to that of the applied electric and magnetic field directions, which reveals the existence of the electric field drift in the system under study. We also use an oblique force field as the external driving force, both in the presence and absence of the external magnetic field. The application of this oblique force changes the orientation of the lane structures for different applied oblique angle values.

Key words: plasma simulation, strongly coupled plasmas

1. Introduction

As a field of research, non equilibrium physics is simultaneously very new and very old. Non equilibrium physics is inherently interdisciplinary. It has grown into a major enterprise. Non equilibrium systems that form patterns or exhibit complex behaviors are especially sensitive to small perturbations; thus their detailed behavior may be extremely challenging to predict or control, and as such is therefore a very interesting field of research. Pattern formation is ubiquitous in nature (Cross & Hohenberg 1993); it occurs for instance in systems undergoing convection, in crystals developing in supercooled or supersaturated environments and even in growing biological systems. In gas discharge

† Email address for correspondence: baruah.s1@gmail.com

systems, patterns often can be observed in the glow emitted by the plasma, for example, in direct current discharges with one electrode made of a semiconductor material (Astrov *et al.* 1998; Strümpel, Astrov & Purwins 2002) and in dielectric barrier discharges (Ammelt, Schweng & Purwins 1993; Breazeal, Flynn & Gwinn 1995). Lane formation (Sarma, Baruah & Ganesh 2020) is another representative example of non-equilibrium phase transition. When two kinds of particles are driven in opposite directions, the system exhibits a self-organization from a uniformly mixed state into strongly ordered anisotropic patterns. This driven segregation phenomenon, first found in computer simulations (Dzubiella, Hoffmann & Löwen 2002; Sarma *et al.* 2020) has been observed in laboratory experiments, such as mixtures of oppositely charged colloids (Leunissen *et al.* 2005*a*) or dusty plasmas in the presence of an external electric field (Sütterlin *et al.* 2009). For a fundamental understanding of such non-equilibrium phenomena requires the study of non-equilibrium phase transition phenomena from 'first principle' approach, such as Molecular Dynamics (MD) simulation, which integrates N particle system without any ansatz or assumptions (Sarma *et al.* 2020).

Phase transitions are common in equilibrium systems, and the related analogies have represented an important contribution to the understanding of non-equilibrium processes. While equilibrium bulk phase transitions are now well understood both by computer simulations (Allen *et al.* 1989) and by statistical theories (Hansen & McDonald 1986; Löwen 1994), non-equilibrium situations may induce a much richer scenario of phase transformations. Until now, very extensive theoretical and simulation studies have been performed on such transitions in driven diffusive systems (Katz, Lebowitz & Spohn 1983; Marro & Dickman 1999), particularly, models of identical particles have been studied, which couple with a different sign to an external uniform field (Aertsens & Naudts 1991), and the particles then form stripes perpendicular to the field direction. Later, this transition has been put forward as a concept of panic theory applied to pedestrian zones (Helbing, Farkas & Vicsek 2000). Similar situations with two groups of particles moving in the other direction have been extensively studied in the context of lane and pattern formations not only of pedestrians (Ikeda & Kim 2017; Feliciani, Murakami & Nishinari 2018), but also of various physical particles, such as charged colloids (Vissers *et al.* 2011*b*; Vissers, van Blaaderen & Imhof 2011*a*; Tarama, Egelhaaf & Löwen 2019), granular systems (Aranson & Tsimring 2006), migrating macroions (Netz 2003), microswimmers (Kogler & Klapp 2015) and plasmas (Sarma *et al.* 2020). However, the mechanism of phase transition is much less clear for non-equilibrium conditions. Additionally, the phase stability of pair plasmas in the strongly coupled regime has attracted special attention. In realization of the fact, Swati Baruah *et al.* (Baruah, Ganesh & Avinash 2015) carried out investigations for addressing phase transitional study in strongly coupled two-dimensional (2-D) pair-ion plasma (PIP) system with a soft core. Furthermore, our recent work on a self-organization effect (Sarma *et al.* 2020) where the 'plasma' is structured as a set of lanes that alternatively contain positive and negative ions provides an opportunity for the in-depth fundamental understanding of non-equilibrium lane formation phenomena in the naturally occurring PIP systems.

PIP is a novel state of multi-ion plasma. This kind of plasma is made up of opposite charges and equal masses. The PIPs represent an interesting state of matter with unique thermodynamic properties drastically different from ordinary electron–ion plasmas (Iwamoto 1993). The PIP plays a significant role in plasma physics, for example, numerous astrophysical environments such as the pulsar magnetosphere, active galactic nuclei, neutron stars, etc. (Piran 2005), where intense energies create electrons and positrons through pair production and annihilation. In the last few years, a lot of research work has been performed to explore the linear as well as nonlinear properties of PIPs so as to

https://doi.org/10.1017/S0022377821000027 Published online by Cambridge University Press

understand such types of astrophysical plasmas (Sahu *et al.* 2015). In semiconductors, non-thermal pair plasmas are ubiquitous in the form of electron and ion holes (Piran 2005). The PIP is expected to be used for the synthesis of dimers directly from carbon allotropes, as well as for nanotechnology (Oohara & Hatakeyama 2003*a*). The physics of the PIP became more interesting when its application extended to the terrestrial laboratory. Generally, attention has been focused largely on the relativistic and weakly relativistic regime (Iwamoto 1993; Zank & Greaves 1995; Asseo 2003) of PIP, since such plasmas are thought to be generated naturally under certain astrophysical conditions (Asseo 2003). In many of the cases above, magnetic fields – static as well as dynamic fields – are known to play an important role (Pilch *et al.* 2007; Pilch, Reichstein & Piel 2008; Baruah & Das 2010; Ott & Bonitz 2011). In PIPs, pair annihilation can take place (Zank & Greaves 1995). This process is analogous to recombination in electron–ion plasmas. Another interesting fact is that in such plasmas the nonlinear phenomena such as solitary wave structures in stationary plasmas and in the beam plasma system, cross-field transport, and the phenomena of holes and clumps are different from electron–ion plasmas (Berman, Tetreault & Dupree 1985). Many of the phenomena found in conventional electron–ion plasmas exist in modified form, while others, notably the whistler wave, the lower hybrid wave and Faraday rotation, are absent (Zank & Greaves 1995).

A number of experimental approaches have been proposed for studying PIP in the laboratory, and a few of them are now being actively pursued. Oohara & Hatakeyama (2003*b*, 2007) reported that fullerene PIP $C_{60}^{\pm}$ can be produced experimentally. Further, electron-free, positive and negative-ion plasmas have been achieved in the afterglow of pulsed-power Cl_2 discharges (Kanakasabapathy & Overzet 1998), and some control on the amount of background electron population has also been achieved. Remaining very low density background electrons tend to play the role of 'shielding'. Recently, in another experimental work, PIP with positive and negative Hydrogen ions ($H^+ + H^-$) has been successfully created (Oohara & Hatakeyama 2007). In this work, it is assumed that pair-ions interact with a potential which is of Yukawa form, where the shielding of the PIP particles is believed to come from the 'background' electrons, as observed in the $C_{60}^{\pm}$ experiment (Oohara, Date & Hatakeyama 2005).

It is well proven that an external magnetic field influences the dynamics of the charged particles as well as their collective behaviour in plasma systems. Over the last decade, a series of research focusing on the effect of the externally applied magnetic field over the particle dynamics has been reported. For example, dusty plasma offers an excellent medium for studying various phenomena at single particle and fluid levels with remarkable temporal and spatial resolutions in the presence of an external magnetic field. An experimental study of fine particles in magnetized plasma was done by Sato *et al.* (2001). They found that fine particles rotate in the azimuthal direction on the horizontal plane in presence of a magnetic field applied in the vertical direction. In their experiment, the rotation is induced under the condition that the particles are strongly coupled with very small interparticle distance. Konopka *et al.* (2000) studied the effect of a vertical magnetic field on the particle cloud in the sheath of a radio frequency He plasma at various discharge conditions. They observed that the cloud rotates under the influence of the magnetic field. Uchida, Konopka & Morfill (2004) on the other hand, studied the wave dispersion relation in a 2-D strongly coupled plasma crystal by using both theoretical analysis and MD simulation, taking into account a constant magnetic field parallel to the crystal normal. Very recently, a dusty plasma device capable of operating with magnetized electrons, ions and charged dust particles was designed at Auburn University, USA, under the direction of Thomas *et al.* (2019), to study of highly magnetized plasmas and dusty plasmas, where, experiments can be performed at magnetic field up to 4T. Their study

https://doi.org/10.1017/S0022377821000027 Published online by Cambridge University Press

shows the formation of new types of self- and imposed-ordered structures that form in both plasma and among the microparticles.

The PIP in a magnetic field is unique in that both species are equally and strongly magnetized (Zank & Greaves 1995). Additionally, the behaviour of such a kind of plasma system in the presence of the external magnetic field in 2-D is largely unexplored. Therefore, here, we focus on a 2-D PIP system and explore the lane formation dynamics, using computer simulations, under the influence of an external magnetic field. Here, the entire work is performed for $\kappa \sim 0$ ($\kappa = 10^{-4}$), where, $\kappa = a/\lambda_D$ is the screening parameter resulting from the shielding dynamics of 'background' charged particles (Sarma *et al.* 2020), λ_D is the Debye length and 'a' is the Wigner–Seitz radius; for the rest of the presentation this is the value of κ used. In this study, the particle motion is governed by Langevin dynamics (LD). In our previous work (Sarma *et al.* 2020), lane formation dynamics of driven 2-D PIPs were investigated in the underdamped case, where we studied the behaviour of the system in the presence of both constant and time-varying external electric field taking into consideration the finite screening case ($\kappa \neq 0$). There, comparative study performed between the results in the overdamped and underdamped limit brought new and interesting information as far as the self-organization effect is concerned. Here, we focus on some aspects of the lane formation dynamics of a PIP system in a magnetic field in the presence of both constant and oscillatory electric fields in zero κ limit. First we perform our study by applying the external electric field (both constant and oscillatory) in the Y-direction, considering the external magnetic field direction is out of the simulation chamber, and obtain the critical value of the strength of the external electric field above which lanes are formed distinctly in the presence of the external magnetic field. The resulting critical electric field strength is then compared with the one in the absence of the external magnetic field and it is observed that the presence of the external magnetic field retards the phase transition process and leads to a disintegration of lane formation. Through this present study, we expect that our results may provide an opportunity for an in-depth fundamental understanding of non-equilibrium lane formation phenomenon in the naturally occurring PIP systems as well as for their relevance to technological applications. Additionally, due to the appearance of electric field ($E \times B$) drift in our system, the self-organized lanes start to move along a direction perpendicular to both the directions of the applied electric and magnetic fields. It is also observed that the self-organization is correlated to a strong decrease of the transverse diffusion coefficient in the absence of the external magnetic field. However, due to the appearance of the electric field drift, the value of the long-time self-diffusion coefficient increases along with the electric field strength after getting into the self-organized phase. On the other hand, from a Coulomb coupling parameter varying order parameter plot we observed the existence of a lane formation-disintegration phase of the PIP system both in the presence and absence of the external magnetic field, taking into consideration of the constant electric field case, which reveals that, in our system, a range of critical coupling parameters exists in which only the system shows a self-organized phase.

Using Langevin Dynamics (LD) simulation technique, we further demonstrate the existence of a non-stationary lane-like self-organization behaviour, with oscillation between self-organized and random states for the small frequency values, when submitted to a time-varying electric field and,as a result of the guiding centre drift, lanes are found to move along a direction perpendicular to both the electric and magnetic field directions. It is also seen that, for each electric field there exists a critical frequency above which the system cannot reach the self-organized state and the presence of the external magnetic field significantly affects the critical frequency value. However, in second part of the paper we discuss the results obtained from the application of the oblique external electric field (both

https://doi.org/10.1017/S0022377821000027 Published online by Cambridge University Press

constant and oscillatory field) to the PIP system in the presence of the external magnetic field. Our motivation for studying a PIP system comes from the fact that the magnetic field may affect the lane formation dynamics of these particle species differently. On the other hand, phase transitions in conventional and model complex fluids are of significant scientific and technological interest. The phase transition mechanism in a driven system reveals a wealth of novel instabilities and pattern formations induced by non-equilibrium conditions (Sarma *et al.* 2020). However, a complete understanding of the key parameters which determine the existence and order of non-equilibrium phases still remains to be explored fully in a PIP system and is an active area of research. Additionally, the behaviour of such a kind of plasma system in the presence of the external magnetic field in two dimensions is largely unexplored. Therefore, for this study we have chosen a pair-ion system to explore the lane formation dynamics, using computer simulations, under the influence of an external magnetic field.

The rest of the paper is organized as follows: In § 2, we define the model used. The simulation technique, along with the lane formation order parameter and long-time self-diffusion coefficient, are discussed in § 3. In § 4, the results are presented and discussed in detail. Finally we finish with conclusions in § 5.

2. The model

We simulate the Langevin molecular dynamics for a 2-D PIP system of N charged particles in a regular square of length $X = Y = L$ keeping the total density ρ and the temperature constant. The periodic boundary condition is used in both the X and Y-directions. Here, half of the PIP particles carry positive charge and the other half carry a negative charge of the same magnitude $|Q|$ and of equal masses subjected to a perpendicular external magnetic field $\boldsymbol{B} = B\hat{e}_z$ ($\hat{e}_z$ is the unit vector along Z-direction). The number density is $\rho = N/L^2$, where L is the dimension of the system.

The particle trajectories are governed by the LD

$$m_i \frac{\mathrm{d}^2 \boldsymbol{r}_i}{\mathrm{d}t^2} = -\gamma \frac{\mathrm{d}\boldsymbol{r}_i}{\mathrm{d}t} - \sum_{i<j} \boldsymbol{\nabla} U(r_{ij}) + \boldsymbol{F}_{\mathrm{ext}} + \boldsymbol{F}_i^{(R)}, \tag{2.1}$$

where $i = 1, \ldots, N$, m_i, r_i are, respectively, the number of PIP particles, the mass and position of the ith particle, $-\sum_{i<j} \boldsymbol{\nabla} U(r_{ij})$ is the force comprised of interparticle interactions. As is well known, in Langevin model, each PIP particle experiences a Brownian motion from the background interactions which results in dissipation of PIP particles via $-\gamma(\mathrm{d}\boldsymbol{r}_i/\mathrm{d}t)$, here γ is the friction constant. The force, comprised of the external force fields, is

$$\boldsymbol{F}_{\mathrm{ext}} = \boldsymbol{F}_E + \boldsymbol{F}_B, \tag{2.2}$$

were $\boldsymbol{F}_E$ is the space-independent external electric force acting on the particles pointing in the Y-direction, and is modelled as

$$\boldsymbol{F}_E(t) = \hat{y} E_0 \cos(\omega t) \tag{2.3}$$

where E_0 is the strength or amplitude of the external electric field, ω is the frequency of the external electric field (with $\omega \equiv 0$ leading to the constant-field case) and $\hat{y}$ is the unit vector along the Y-direction. Temporally oscillatory electric fields are often found both in experiments (either controlled form or in noise form) and in other naturally occurring PIPs, such as in active galactic nuclei (Begelman, Blandford & Rees 1984), in stars (Michel 1991), in pulsar magnetospheres (Paul N. Arendt & Eilek 2002), in gamma ray fire balls

https://doi.org/10.1017/S0022377821000027 Published online by Cambridge University Press

(Piran 1999), in solar flares (Tandberg-Hanssen & Emslie 1988), etc. As is well known, any bounded function $f(t)$ may be represented as aFourier sum of frequencies ω and their appropriate weights. Thus, performing numerical studies with a cosine or sine function of ω (see (2.3)) should be able to give generic insight for either a controlled or noise form of external electric field. Additionally, as the occurrence of lane formation appears to be very general, this non-equilibrium transition could be experimentally verified in quite different systems (2001) as well as observable in real systems, e.g. driven by an oscillatory electric field. Hence, in our case, for a fundamental understanding of the lane formation phenomenon occurs in realistic system (here, in a naturally occurring PIP system), the electric field is modelled as mentioned in (2.3). The force due to the external magnetic field applied along the Z-direction (i.e. out of the simulation box) is

$$\boldsymbol{F}_B = \frac{Q_{A,B}B}{m_i c}\dot{r}_i \times \hat{e}_z, \tag{2.4}$$

where c is the speed of light. The force $\boldsymbol{F}_i^{(R)}$ describes random kicks of the background acting on the ith PIP particle by the 'bath'. These kicks are mimicked by Gaussian random numbers with zero mean, $\overline{\boldsymbol{F}_i^{(R)}} = 0$, and variance

$$\overline{(\boldsymbol{F}_i^{(R)})_\alpha(t)(\boldsymbol{F}_j^{(R)})_\eta(t')} = 2k_BT\gamma\delta_{\alpha\eta}\delta_{ij}\delta(t-t'). \tag{2.5}$$

The subscripts α and η stand for two Cartesian components, i and j stands for ith and jth particles, t and t' for two distinct time, where the first and second δ are Kronecker and the third δ stand for Dirac delta function and k_BT is the thermal energy of the bath.

The interaction potential reads as

$$U(r_{ij}) = \left(\frac{Q_AQ_B}{4\pi\epsilon_0 r_{ij}}\right)\exp\left(-\kappa\left(\frac{r_{ij}}{a}-1\right)\right), \tag{2.6}$$

where, r_{ij} is the distance between ith and jth pair, $Q_{A,B}$ is the charge of particle A (B), such that $Q_AQ_B = -1$ and $Q_AQ_A = Q_BQ_B = +1$. This is a valid model for charge-stabilized suspensions in three (Löwen & Kramposthuber 1993) and two (Lowen 1992) spatial dimensions. It has also been shown experimentally that the potential as mentioned above ((2.6), i.e. Yukawa potential) is a suitable effective interaction for this kind of system (Leunissen *et al.* 2005*b*; Royall *et al.* 2006). Here, the length, time, energy, density and electric field are normalized, respectively, by a, ω_p^{-1}, k_BT, a^2 and $Q/4\pi\epsilon_0a^2$. In these units, the strength of the interaction potential is defined as Γ, where $\Gamma = Q_{A,B}^2/4\pi\epsilon_0ak_BT$; here, k_BT denotes the thermal energy. In this study, the strength of the magnetic field B is given by $\beta = \omega_c/\omega_p \propto B$, i.e. the ratio of the cyclotron frequency $\omega_c = Q_{A,B}B/m_ic$ (here, c represents speed of light) and the plasma frequency $\omega_p = [2Q_{A,B}^2/4\pi\epsilon_0a^3m_i]^{1/2}$. Here '$a$' is the Wigner–Seitz radius, ϵ_0 is the permittivity of free space and $Q_{A,B}$ is the charge of particle $A(B)$. Here, simulations are performed with β values varying from 0.001 to 1.0. In real units, $\beta = 1.0$ is equivalent to magnetic field strength $B = 4.6388$ T for the PIP system as created in the $C_{60}^{\pm}$ experiment (Oohara *et al.* 2005). As mentioned in the introductory section above, already experimental works (Thomas *et al.* 2019) are going on where highly magnetic fields with strength 4 to 5 T are used; therefore, the range of magnetic field strength that is used in this study can be considered as reasonable enough to describe this problem.

https://doi.org/10.1017/S0022377821000027 Published online by Cambridge University Press

For this study, the stochastic Langevin normalized equations for the particle trajectories $\boldsymbol{r}_i(t)$ $(i = 1, \ldots, N)$ read as

$$\frac{\mathrm{d}^2\boldsymbol{r}_i}{\mathrm{d}t^2} = -\gamma\frac{\mathrm{d}\boldsymbol{r}_i}{\mathrm{d}t} + \sum_{i<j}\frac{\Gamma}{r_{ij}}\left(\kappa + \frac{1}{r_{ij}}\right)\exp[-\kappa(r_{ij}-1)] + \boldsymbol{F}_{\mathrm{ext}}(t) + \boldsymbol{F}_i^{(R)}(t). \tag{2.7}$$

In this work, we study two cases in the presence of the external magnetic field: in first case, the external constant or oscillatory electric force $\boldsymbol{F}_E$ is pointing in the Y-direction as discussed in (2.3) above; in second case, the external electric field $E_0\cos(\omega t)$ intersects the X–Y plane at an oblique angle θ. The force due to the oblique electric field reads as

$$\boldsymbol{F}_E = \boldsymbol{F}_{\mathrm{EOblique}} = F_{\mathrm{Ex}}\hat{e}_x + F_{\mathrm{Ey}}\hat{e}_y. \tag{2.8}$$

The corresponding components of the oblique electric field are modelled as

$$\left.\begin{aligned} F_{\mathrm{Ex}} &= E_0\cos(\omega t)\cos(\theta),\\ F_{\mathrm{Ey}} &= E_0\cos(\omega t)\sin(\theta). \end{aligned}\right\} \tag{2.9}$$

3. Simulation procedure

Extensive LD simulations using the OpenMP parallel program are carried out to analyse the effect of the external magnetic field ($\beta \neq 0$) on the non-equilibrium phase transition which is associated with lane formation parallel to the external field of the 2-D PIP. The simulations are performed using $N = 500$ particles in a square simulation cell of side L. In the process of deciding the appropriate number of particles N, we have performed a series of runs from $N = 250$ to 2000 ($N = 250$, 500, 600, 700, 1000 and 2000) at fixed density ρ and found that for particles $N \geqslant 500$, the finite size effects tend to become negligible. Hence $N = 500$ has been chosen for this study (Sarma *et al.* 2020). After equilibration with the desired temperature Γ^{-1}, using the Langevin equation, the force due to the external electric field $\boldsymbol{F}_E$ is applied to the particles. Here, the external magnetic field is applied from the beginning of the simulation until the entire study has been performed. The lane or structure order parameter (defined later) is evaluated for various values of the applied electric field strength E_0 in the presence of the external magnetic field. As shown earlier (Sarma *et al.* 2020), here also it is found that beyond a critical value of E_0, the order parameter tends to unity. It is also observed that the critical electric field strength value obtained from our simulations is independent of the system size, which suggests that $N = 500$ is enough to describe this problem and to minimize the finite size effect.

To begin with, each particle is assigned an initial velocity which is random in direction, such that the average kinetic energy corresponds to the chosen temperature. The Langevin equations of motion including the external electric and magnetic fields are solved using the velocity Verlet method with a sufficiently small time step Δt. The simulation is done in the following steps.

For both the constant and oscillatory field cases including the oblique force field cases, with and without the external magnetic field (for a typical run, say, at $\Gamma = 2.5$, $\rho = 0.5$) typically $8 \times 10^5\Delta t$ steps are simulated which corresponds to a simulation time of $t\omega_{\mathrm{pd}} = 2400$ with $\Delta t = 3 \times 10^{-3}$. After equilibration with the thermal energy using the Langevin equation, the external force field is applied to the particles at a time $t = 2 \times 10^5\Delta t$ steps. The data collection is obtained for the last $2 \times 10^5\Delta t$ steps after the system has reached a far-from-equilibrium quasi-steady-state.

https://doi.org/10.1017/S0022377821000027 Published online by Cambridge University Press

3.1. *Order parameter*

To characterize the degree of lane formation, a convenient order parameter is proposed for evaluating the number of particles of the same species along the driven direction (the Y-direction here). An order parameter in effect counts the percentage of particles in a lane-like configuration. It helps to distinguish two different phases (or orders) (Sarma *et al.* 2020). For example, in one phase, the value of the order parameter may be zero and in another phase it may attain a non-zero value. Following Ikeda & Kim (2017) and Sarma *et al.* (2020), we define the following as the order parameter of lane formation. The simulation system is divided into $n_{\rm div}$ numbers of identical rectangular strips along the driven direction (i.e. along $\hat{y}$). Thus, the width of each strip along the x-direction is given by $l_{\rm div} = L/n_{\rm div}$. The order parameter for the lane formation, say, in the kth strip (ϕ_k) is determined by the difference in numbers between the positively and negatively driven particles, which is normalized by the total particle number in the k-th strip as

$$\phi_k = \frac{n_k^+ - n_k^-}{n_k^+ + n_k^-}, \tag{3.1}$$

where $n_k^{\pm}$ represents the number of '$\pm$' species in the kth rectangular strip. Thus, the range of ϕ_k is from -1 to 1, and it becomes positive if the positive particles become dominant in the strip, and negative if the negative particles become dominant. The order parameter ϕ for the total system is then defined as

$$\phi = \left\langle \frac{1}{n_{\rm div}} \sum_{k=1}^{n_{\rm div}} \mid \phi_k \mid \right\rangle, \tag{3.2}$$

where the bracket denotes a time average. The order parameter ϕ begins at around 0 at the initial state since oppositely charged particles are found inside the system, and finally reaches 1 when the system exhibits the lane formation in the steady state. The former corresponds to the randomly mixed state, whereas the latter corresponds to the lane formation structure by the particles of the same species along the driven direction. We note that our definition of ϕ is essentially the same as those introduced previously (Dzubiella *et al.* 2002; Ikeda, Wada & Hayakawa 2012; Sarma *et al.* 2020).

3.2. *Long-time self-diffusion coefficient (D_{xL})*

The long-time self-diffusion coefficient $D_{\rm xL}$ perpendicular to the external field direction is defined as (Sarma *et al.* 2020)

$$D_{\rm xL} = \lim_{t\to\infty} \frac{1}{2t} \left\langle \sum_{i=1}^{N} [(r_i(t) - r_i(0)) \cdot \hat{x}]^2 \right\rangle, \tag{3.3}$$

where $r_i(t)$ is the trajectory of the ith particle at an instant t. Here, $\langle \ldots \rangle$ is the equilibrium average for a system unperturbed by the external force.

The calculation of the long-time self-diffusion coefficient $D_{\rm xL}$ perpendicular to the applied field direction will help us to distinguish between the mixed orderless state and lane state (Sarma *et al.* 2020). The details of the working of the long-time self-diffusion coefficient $D_{\rm xL}$ in this context is discussed in the § 4.

4. Results and discussions

In this paper, we perform our study to see the effect of an external magnetic field on lane formation dynamics in PIP using both constant and oscillatory external electric fields

https://doi.org/10.1017/S0022377821000027 Published online by Cambridge University Press

using the Langevin equation of motion (2.1). This work will primarily focus on finding out the parameter regime of existence of lane structures in a PIP system in the zero screening limit in the presence of the external magnetic field and details of it is discussed in § 4.1. From the comparative study between the results obtained from the presence and absence of the external magnetic field it is observed that a higher value of the electric field strength (constant field case) will be needed to enter into the lane formation regime in the presence of the external magnetic field, however, comparatively at a lower value of the electric field frequency (known as the critical frequency for oscillatory field case), the system exhibits a transition back to the disordered state in the presence of the external magnetic field. The paper will then discuss how this lane formation mechanism will be significant in the presence of the oblique external electric field both in the presence and absence of the external magnetic field in § 4.2.

4.1. *Lane formation in the presence of the external magnetic field ($\beta \neq 0$)*

4.1.1. *Constant field*

In this subsection, we report on comprehensive simulation studies of lane formation in a PIP system, that are carried out in the presence of a constant external electric field. Here, we focus the influence of the external magnetic field on the lane dynamics. The magnetic field is applied from the beginning of the simulation in every case being studied.

Three simulation snapshots in the steady state for increasing external electric forces and with $\beta = 1.0$ are shown in figure 1. Figure 1 shows the simulation snapshots associated with a situation with an external electric field below the critical field point (E_c), at the critical field point and above the critical field strength, in the presence of the external magnetic field ($\beta = 1.0$). As shown earlier (Sarma *et al.* 2020) for the finite κ and $\beta = 0$ case, in this study one also clearly sees lane formation parallel to the external electric field in the presence of the external magnetic field. These figures indicate that large E_0 leads to lane formation. With increasing E_0, the collision between oppositely driven particles was enhanced. This effect resulted in a bundle of particles in the same direction and generated the interface between oppositely driven particles; this is the main mechanism for the lane formation. From figure 1, it is seen that the thickness of the lanes perpendicular to the driven direction involve several particle layers for the external field strength $E_0 > E_c$ and is comparable to the size of the simulation box. This implies that lane formation is a macrophase separation. However, below the critical strength needed to generate lane formation, some very weak patterns are generated with a width of one particle. Moreover, it is also observed that due to the presence of both uniform electric and magnetic fields the PIP particles experience not only the usual circular Larmor gyration, but also a drift of the guiding centre ($E \times B$ or electric field drift), and as a result of which the lanes seem to move along the X-direction of the simulation chamber. As the magnitude of this electric field drift of the guiding centre is generally defined as $v_E = E_0/B$, therefore, from our simulation results it is observed that with increasing electric field strength E_0 the movement of the lanes towards the X-direction increases. In order to characterize the degree of lane formation in the presence of an external magnetic field ($\beta = 1.0$), the order parameter (ϕ) is calculated for various values of the electric field strength (E_0) ranging from 1.0 to 200, taking density value ($\rho = 1.0$) as shown in figure 2, both in the presence ($\beta = 1.0$) and absence ($\beta = 0.0$) of the external magnetic field. In real units, the above-mentioned range of E_0 examined here are equivalent to $E_0 \approx$ 14.405 to 2881.133 volts per metre, for the PIP system as created in the $C_{60}^{\pm}$ experiment (Oohara *et al.* 2005). It is observed that, for both the cases, ϕ is small for a smaller value of field strength, and it grows when a critical electric field strength (E_c) is approached. As observed, with turning on the external field strength E_0, PIP particles only follow the

https://doi.org/10.1017/S0022377821000027 Published online by Cambridge University Press

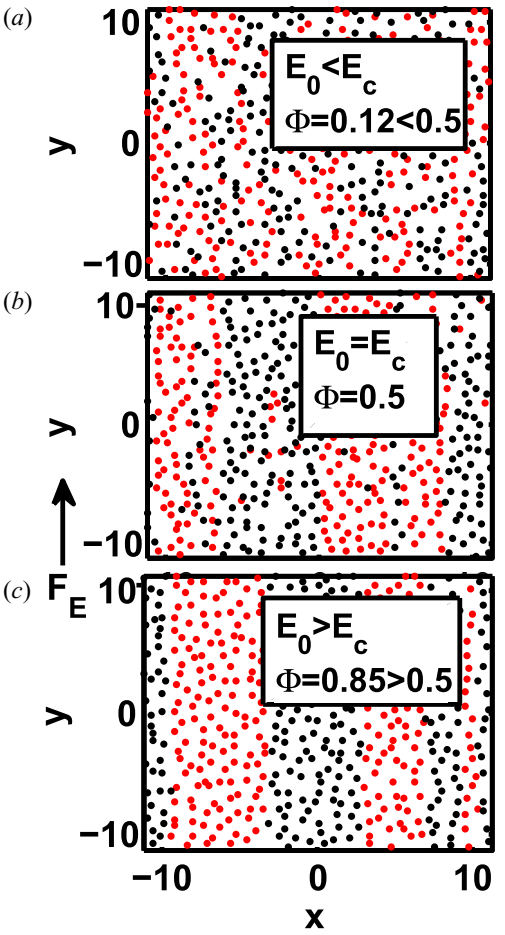

FIGURE 1. Typical simulation snapshots of the 2-D PIP system with constant external electric field ($\omega = 0$), taking $\beta = 1.0$, $\Gamma = 2.5$, $\rho = 1.0$. Panel (a) shows disordered state with electric field $E_0 < E_c$ ($\phi = 0.12 < 0.5$), panel (b) shows a less disordered state with electric field $E_0 = E_c$ ($\phi = 0.5$) and panel (c), shows ordered lane formation with $E_0 > E_c$ ($\phi = 0.85 > 0.5$).

external field by eluding each other, so that the diffusion perpendicular to the external field has to increase with E_0. This effect grows until the critical field strength is reached and the system begins to form lanes. The critical value of the electric field strength E_c is determined at the electric field strength value where the generation of lane formation has just started, and the corresponding value of the order parameter is recorded as $\phi = 0.5$ for the simulation runs with increasing field strength. It is noted that this particular value is also considered as the threshold value to characterize the critical lane value by other authors (Dzubiella *et al.* 2002; Rex & Löwen 2008; Klymko, Geissler & Whitelam 2016; Ikeda & Kim 2017; Sarma *et al.* 2020). Thus, the value $\phi = 0.5$ plays a significant role in identifying the phase transition point. The critical field strength E_c thus obtained in the presence of the external magnetic field ($\beta = 1.0$) is $E_c = 70$. However, the location of the phase transition in the absence of the external magnetic field ($\beta = 0.0$) is found at electric field strength value $E_c = 60$, which indicates that the presence of the external magnetic field retards the phase transition process, as can be verified from figure 2.

https://doi.org/10.1017/S0022377821000027 Published online by Cambridge University Press

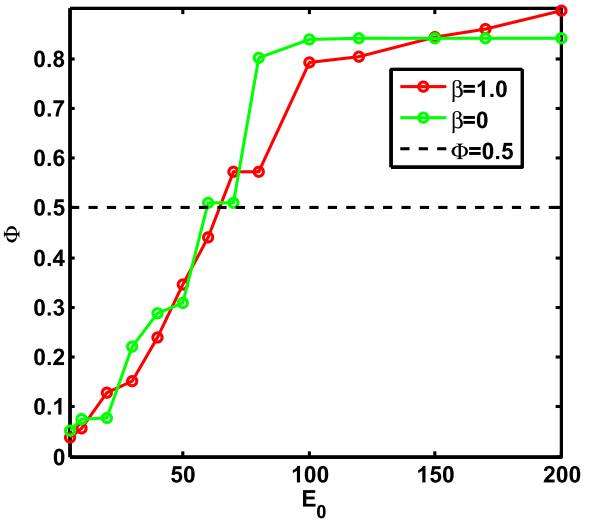

FIGURE 2. Order parameter ϕ versus electric field strength E_0 plot for constant electric field case ($\omega = 0$) both in the presence of the external magnetic field ($\beta = 1.0$) and in the absence of the magnetic field ($\beta = 0.0$), taking other parameters as $\Gamma = 2.5$, $\rho = 1.0$.

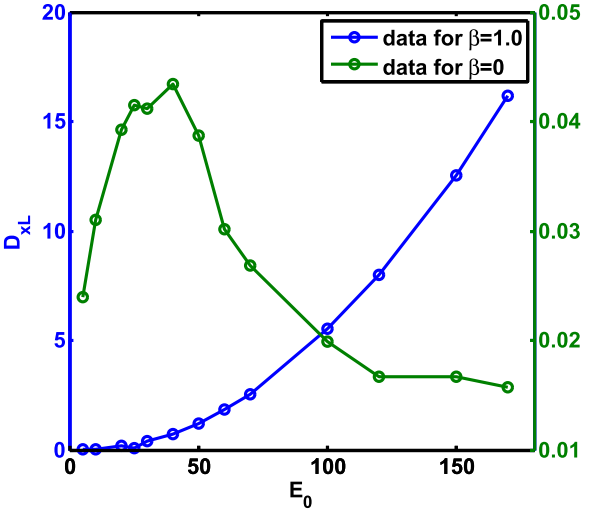

FIGURE 3. Perpendicular diffusion coefficient (D_{xL}) versus E_0 plot for constant external electric field case ($\omega = 0$), both in presence ($\beta = 1.0$) and absence ($\beta = 0$) of the external magnetic field, taking $\Gamma = 2.5$, $\rho = 1.0$.

Here, the long-time self-diffusion coefficient D_{xL} is studied along $\hat{x}$, i.e. in the direction perpendicular to both the external electric field (along $\hat{y}$) and magnetic field (along $\hat{z}$). It measures the mean square particle displacement along $\hat{x}$ during a characteristic time interval. Figure 3 shows a comparative plot for the perpendicular long-time self-diffusion coefficient (D_{xL}), both in the presence and absence of the magnetic field, and the other parameters used are $\Gamma = 2.5$, $\rho = 1.0$. The figure clearly signifies the effect of the magnetic field on the diffusion coefficient. In the zero β case, it is observed that the diffusion increases with E_0 and reaches the maximum of D_{xL}, the corresponding E_c is

https://doi.org/10.1017/S0022377821000027 Published online by Cambridge University Press

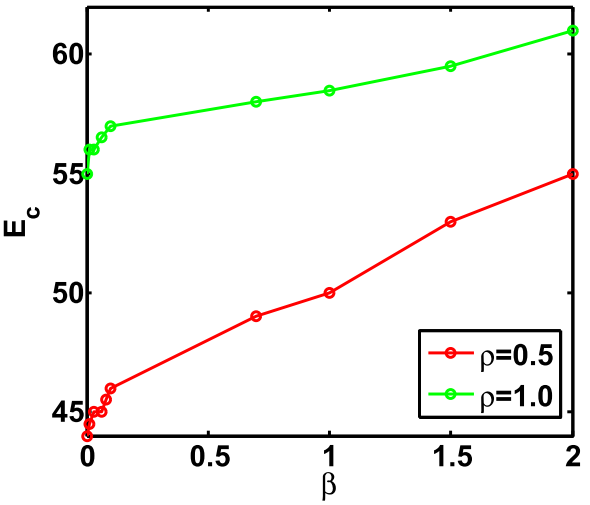

FIGURE 4. Critical electric field E_c versus β plot for constant electric field case ($\omega = 0$), taking $\rho = 0.5, 1.0$, $\Gamma = 2.5$.

found as 50 for the $\beta = 0$ case, where the system begins to form the lanes as indicated by the value of the order parameter $\phi = 0.5$. Now the lateral transport decreases strongly once the particles are in a lane, which reduces the perpendicular diffusion again. As a result, drastic decrease of D_{xL} with E_0 takes place beyond E_c, which strongly indicates the location of the lane formation. However, as indicated in figure 3, unlike the zero β case, for finite β case the value of D_{xL} goes on increasing along with the electric field strength E_0, beyond E_c. This increase in transport perpendicular to the both electric and magnetic field strength indicates the presence of the $E \times B$ drift effect. This may be explained as follows: as the PIP particles tend to move parallel in the direction of the electric field (y-direction) with a certain velocity, they experience a ($E \times B$) drift velocity of magnitude $v_E = E_0/\beta$ (in MD units) due to the presence of both electric field and magnetic field, and as this drift velocity is directly proportional to the electric field strength E_0 and inversely proportional to β, therefore, for a fixed value of β with increasing E_0, drift velocity increases rapidly, which in-turn increases the magnitude of the long-time self-diffusion coefficient as shown in figure 3. However, by modifying the calculation of the self-diffusion coefficient and removing the effect of the $E \times B$ drift velocity (which is not done here), it may be possible to get a similar type of D_{xL} versus E_0 plot as observed for the $\beta = 0$ case.

The phase diagram obtained from a simulation with a constant ($\omega = 0$) external force is shown in figure 4. The location of phase transition is identified as the 'critical field strength E_c' which is obtained by setting $\phi = 0.5$ for a set of runs with increasing E_0. This exercise is performed for different values of the density $\rho = 0.5$, 1.0 and external magnetic field strength (β). An interesting phenomenon observed in this study is that the critical value of electric field strength E_c increases with the application of the magnetic field (β), which indicates that the strength of the external magnetic field also plays an important role in lane formation dynamics. The higher the magnetic field strength, the higher the strength of external electric field required to reach the transition point. From the figure it is also observed that a higher value of the electric field strength (E_c) is required by the system to enter into the lane formation state with an increasing value of the number density of the system in the presence of the magnetic field.

https://doi.org/10.1017/S0022377821000027 Published online by Cambridge University Press

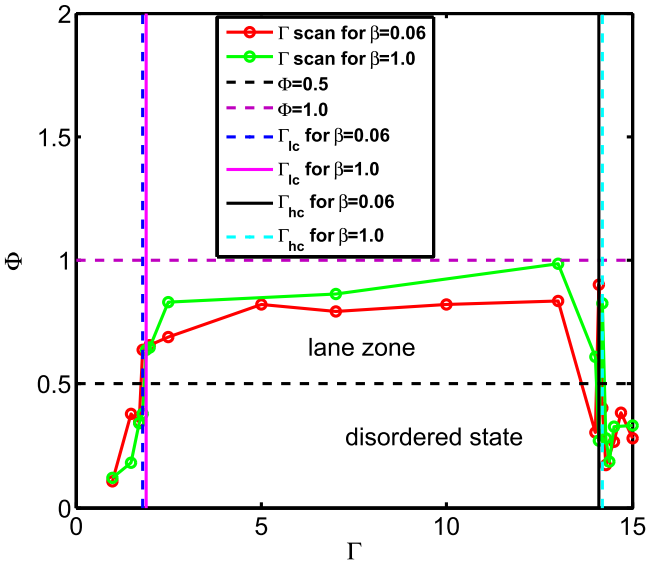

FIGURE 5. Phase diagram for constant electric field case ($\omega = 0$) in the presence of the external magnetic field; location of the phase diagram is estimated via the behaviour of the order parameter for various values of the Γ in the presence of the different magnetic field ($\beta = 0.06, 1.0$). Other parameters are $E_0 = 150$, $\rho = 1.0$, $\Gamma_{\rm lc}$ and $\Gamma_{\rm hc}$, respectively, and indicate lower value of critical limit and higher value of critical limit of Γ. For $\beta = 0.06, 1.0$, $\Gamma_{\rm lc}$ values obtained from simulation are 1.8, 1.9, respectively, and $\Gamma_{\rm hc}$ values are 14.1, 14.2, respectively.

A study related to the dependence of the Coulomb coupling parameter (Γ) on lane formation dynamics is investigated in the presence of the external magnetic field $\beta \neq 0$ in the constant electric field case. Data for the order parameter ϕ which decides the location of phase transition are plotted in figure 5 in the presence of the different values of the external magnetic field ($\beta = 0.06, 1.0$). They are shown versus the Coulomb coupling parameter (Γ). The other parameters used are $E_0 = 150$, $\omega = 0$ and $\rho = 1.0$. The plots clearly show that in the beginning for smaller Γ values, ϕ is small, it grows and reaches $\phi = 0.5$ with increasing Γ, from where the formation of lanes start in the PIP system and that value of Γ is denoted as $\Gamma_{\rm lc}$, the lower limit of critical Γ, which is found as 1.9 for $\beta = 1.0$, and for $\beta = 0.06$, $\Gamma_{\rm lc}$ is found at 1.8. Further increasing the Γ value beyond $\Gamma_{\rm lc}$, the ϕ value grows and gradually reaches unity. This increase in ϕ values gradually reduces and reaches $\phi = 0.5$ again for a Γ value on the higher side, this Γ is indicated as the higher limit of critical Γ, denoted by $\Gamma_{\rm hc}$. However, for further increase in the Γ value beyond $\Gamma_{\rm hc}$, the ϕ value again decreases further. The region between $\Gamma_{\rm lc}$ and $\Gamma_{\rm hc}$ indicates the lane formation regime (where, $0.5 \geqslant \phi \leqslant 1.0$) and this whole trend is observed for both the cases. From our study it is observed that the lane phase extends to a certain Γ range, for $\beta = 1.0$, from $\Gamma_{\rm lc} = 1.9$ (lower limit of critical Γ) to $\Gamma_{\rm hc} = 14.2$ (indicates as higher limit of critical Γ), on the other hand for $\beta = 0.06$ it extends up to $\Gamma_{\rm hc} = 14.1$. Further increase of the Γ value yields ϕ values that decrease gradually as shown in figure 5, indicating the decreasing order of the system. However, at $\Gamma = 14.0$ near phase transition boundary (see, figure 6*a*) a sudden rise of the order parameter value ($\phi = 0.6$) at $t\omega_{\rm pd} = 2400$ is observed indicating a lane ordered state (this can also be understood from the time variation of the ϕ plot (figure 7*a*), along with figure 7*b* for $\beta = 1.0$, the corresponding times when the instantaneous positions of particles are represented), which happens possibly due to

https://doi.org/10.1017/S0022377821000027 Published online by Cambridge University Press

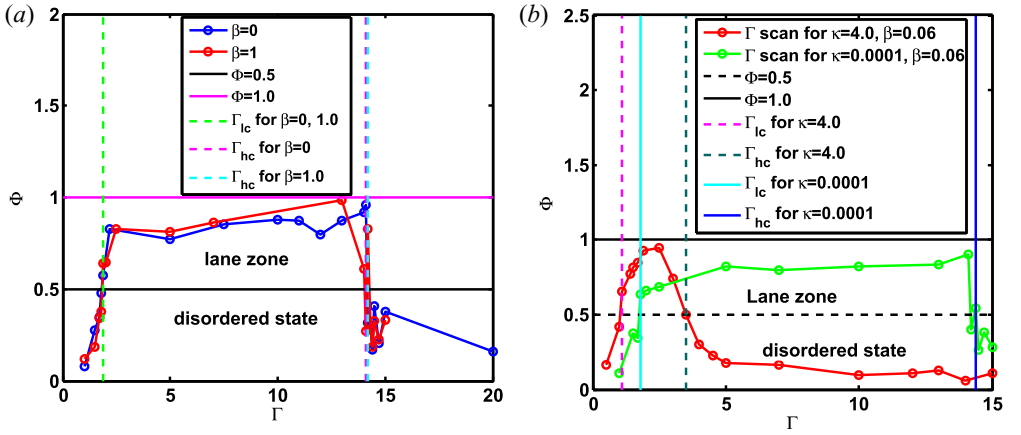

FIGURE 6. Phase diagram indicating ordered lane state and disordered no-lane state. (*a*) Phase diagram for constant electric field case ($\omega = 0$) both in the presence ($\beta = 1.0$) and absence ($\beta = 0$) of the external magnetic field; location of the phase diagram is estimated via the behaviour of the order parameter for various values of the Γ. Other parameters are $E_0 = 150$, $\rho = 1.0$, $\Gamma_{\rm lc}$ and $\Gamma_{\rm hc}$, respectively, which indicate lower value of critical limit and higher value of critical limit of Γ. For $\beta = 0$, $\Gamma_{\rm lc}$ and $\Gamma_{\rm hc}$ are found as 1.9, 14.1, respectively, and for $\beta = 1.0$ $\Gamma_{\rm lc} = 1.9$ and $\Gamma_{\rm hc} = 14.2$ are found. (*b*) Phase diagram for constant electric field case ($\omega = 0$) in the presence of the external magnetic field ($\beta = 0.06$) for both $\kappa = 0.0001, 4.0$; location of the phase diagram is estimated via the behaviour of the order parameter for various values of the Γ. Other parameters are $E_0 = 150$, $\rho = 1.0$, simulated values of $\Gamma_{\rm lc} = 1.1$ and $\Gamma_{\rm hc} = 3.5$, respectively, for $\kappa = 4.0$, and for $\kappa = 0.0001$ $\Gamma_{\rm lc} = 1.8$ and $\Gamma_{\rm hc} = 14.1$ are observed. Here $\Gamma_{\rm lc}$ indicates the lower value of critical limit and $\Gamma_{\rm hv}$ indicates the higher value of critical limit of Γ.

the reason that, near phase boundary there is some discontinuity in free energy takes place. Later, at some points beyond $\Gamma_{\rm hc}$, the system again transits to a completely disordered phase (see ϕ versus $t\omega_{\rm pd}$ plots along with the instantaneous particles snapshots in figures 9, 10, respectively, for $\Gamma = 14.1, 15$). In addition to this, at $\Gamma = 14.2$ for $\beta = 1.0$, the system shows a very peculiar behaviour, in which it again suddenly transfers to the lane state with $\phi = 0.82$ (see figure 11; the physics is not understood), however, beyond that point the system again transits to a disordered state with $\Gamma = 15$ (see figure 10). The behaviour of the 2-D PIP system during the Γ scan in the presence of the different values of the external magnetic field ($\beta = 0.06, 1.0$) may be recognized as the lane formation-disintegration phase. In figure 8, we represent a sequence of snapshots that illustrate this evolution for $\beta = 1.0$.

The lane formation–disintegration phase has also been recognized in our PIP system in the absence of the external magnetic field as shown in figure 6(*a*), where the Γ variation of the order parameter (ϕ) values in the absence of the external magnetic field ($\beta = 0.0$) are plotted with that of the results obtained in the presence of the external magnetic field. For the $\beta = 0$ case, $\Gamma_{\rm lc}$ and $\Gamma_{\rm hc}$ are observed as 1.9, 14.1, respectively, and for $\beta = 1.0$, $\Gamma_{\rm lc}$ and $\Gamma_{\rm hc}$ read as 1.9 and 14.2, respectively. The lane formation–disintegration phase diagram is also plotted for the finite κ case ($\kappa = 4.0$), as shown in figure 6(*b*), in the presence of the external magnetic field strength $\beta = 0.06$ and compared the same with that of the zero κ case in order to see the effect of screening on the lane disintegration process. The finite κ case is studied only for comparison, as the potential used in this study is not accurate for the finite κ case. From our study it is observed that for the finite κ case, the lane formation area shrinks to a smaller region as compared with that of the

https://doi.org/10.1017/S0022377821000027 Published online by Cambridge University Press

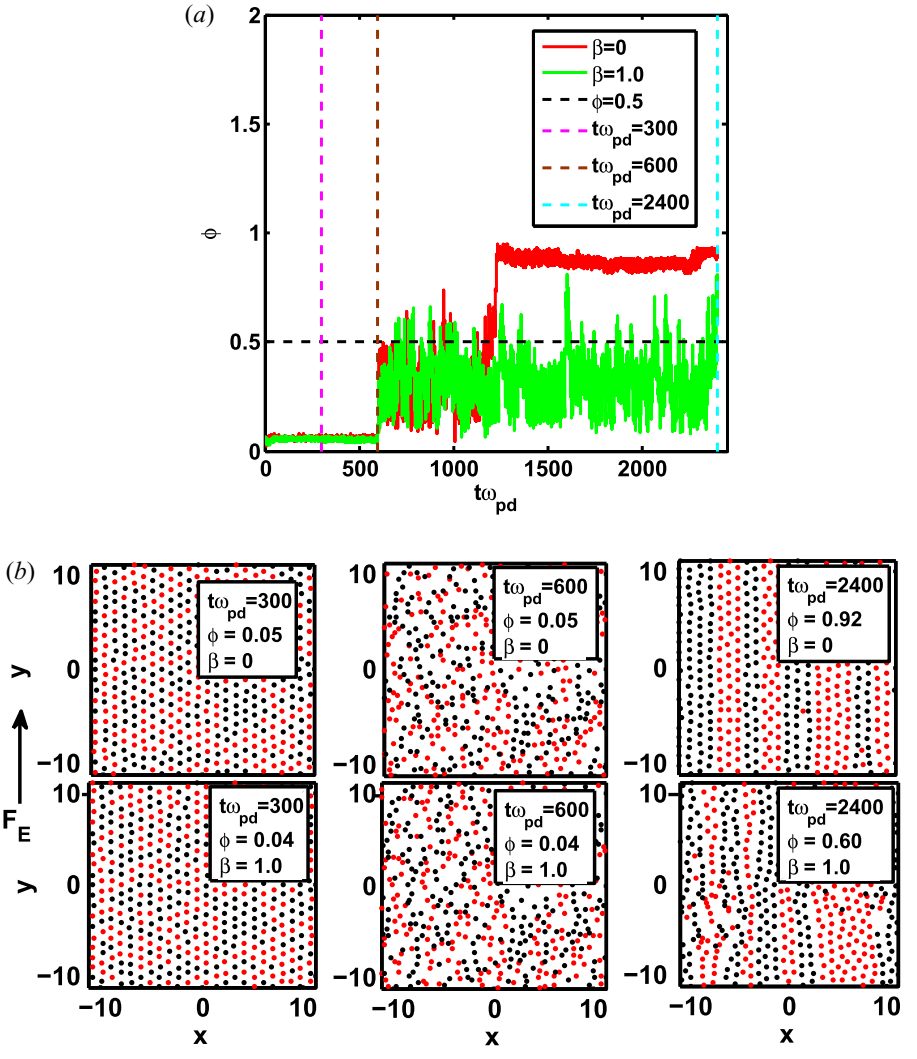

FIGURE 7. Lane formation dynamics both in the presence and absence of the external magnetic field for constant electric field cases. (*a*) Order parameter ϕ versus $t\omega_{\rm pd}$ plot for constant field case, both in the presence ($\beta = 1.0$) and absence ($\beta = 0.0$) of the external magnetic field. Here, electric field is applied at $t\omega_{\rm pd} = 600$ time step. The vertical dashed lines indicate the time at which the simulation snapshots are collected and plotted, as shown in figure 7(*b*). The other parameters used are $E_0 = 150$, $\Gamma = 14.0$ and $\rho = 1.0$. (*b*) Typical simulation snapshots taken at $t\omega_{\rm pd} = 300, 600, 2400$, showing lane formation dynamics in the constant electric field case, both in the presence ($\beta = 1.0$) and absence ($\beta = 0.0$) of the external magnetic field. The other parameters used are $E_0 = 150$, $\Gamma = 14.0$ (near phase transition location) and $\rho = 1.0$.

zero κ case, which indicates that the screening parameter has a significant effect on the lane formation–disintegration process. The lane area extends from $\Gamma_{\rm lc} = 1.1$ to $\Gamma_{\rm hc} = 3.5$ for $\kappa = 4.0$, and for $\kappa = 0.0001$, it ranges from $\Gamma_{\rm lc} = 1.8$ to $\Gamma_{\rm hc} = 14.1$. Additionally, from our study it is also been observed that in the absence of the external magnetic field ($\beta = 0$), at $\Gamma = 14.0$ and $\Gamma = 14.1$, as shown in figures 7(*a*) and 9(*a*), respectively, the order parameter value suddenly raises beyond $\phi = 0.5$ at $t\omega_{\rm pd} = 1300, 1000$ time

https://doi.org/10.1017/S0022377821000027 Published online by Cambridge University Press

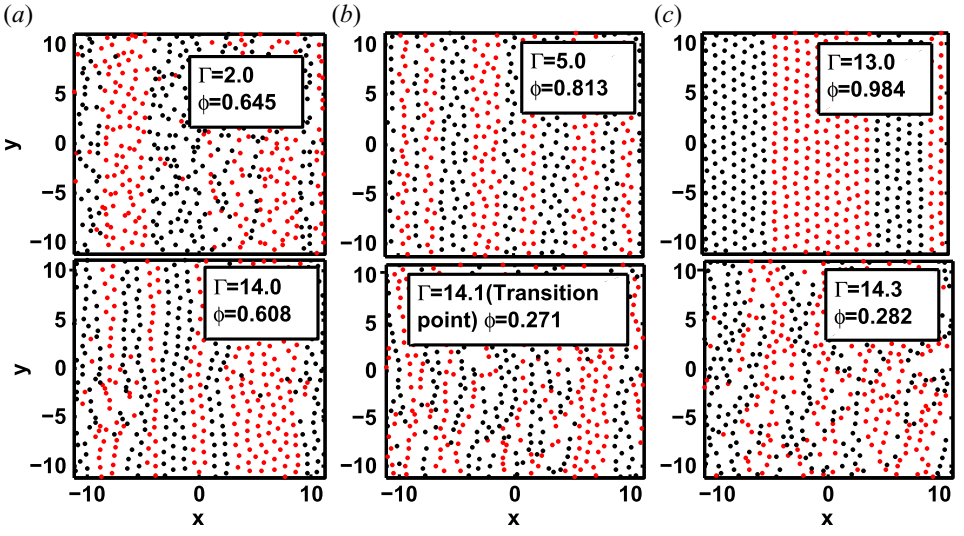

FIGURE 8. Instantaneous positions of particles for different values of Γ for constant electric field ($\omega = 0$) case in the presence of the external magnetic field $\beta = 1.0$, the other parameters used are $E_0 = 150$, $\rho = 1.0$.

steps, respectively, although, the external electric field is applied at $t\omega_{pd} = 600$ time step. However, this behaviour of the order parameter plot in the $\beta = 0$ case is not clearly understood. In addition to that, for both $\beta = 0$ and $\beta \neq 0$ cases, the physical reason behind this lane disintegration process has yet to be understood.

As shown in figures 12(*a*) and 12(*b*), a comparative study on time variation of the order parameter (ϕ) is performed between the $\beta = 0$ case and the $\beta \neq 0$ case (taking different values of the magnetic field strength $\beta = 0.001, 0.005, 0.01, 0.06$) taking $\Gamma = 2.5$ (near the lower limit of the critical Γ value) and $\Gamma = 5.0$ (far from the Γ_{lc}), respectively. Here $\Gamma = 2.5$ taken for figure 12(*a*) is just above the lower value of the critical Γ limit (i.e. $\Gamma_{lc} = 1.9$) both in the presence and absence of the external magnetic field (see, figures 5 and 6*a*) and $\Gamma = 5.0$ used for figure 12(*b*) is far beyond the critical lower limit, (see figures 5 and 6*a*). For all the cases the other input parameters are taken as $E_0 = 150$, $\omega = 0.0$ and $\rho = 1.0$. Here, the magnetic field is applied from the beginning of the simulation, i.e. at $t\omega_{pd} = 0$ time steps, and electric field at $t\omega_{pd} = 600$ time steps. From the ϕ versus $t\omega_{pd}$ plot as shown in figure 12(*b*), taking $\Gamma = 5.0$, an appearance of an oscillatory pattern of the order parameter plots is observed in the presence of the external magnetic field and it increases with an increase in β value. From this plot it is also observed that the frequency of the corresponding oscillation of the order parameter plot increases with an increase in the β value. This result is supported by the frequency (f) of oscillation of the order parameter ϕ versus β plot as shown in figure 12(*c*). This is seen for the whole range of the magnetic field strength under study for $\Gamma = 5.0$. Using a linear fit method, a relation may be obtained between f and β as $f = 0.0076973 + 0.75581\beta$. However, this oscillatory pattern of the time varying order parameter plot is not visible for lower Γ value (i.e. $\Gamma = 2.5$, see figure 12*a*) even with increasing β value. Additionally, in the lower $\Gamma(=2.5)$ case, the order parameter varies in the similar way with time both in the presence and absence of the magnetic field, which is not visible in the presence of a higher $\Gamma(=5.0)$ value.

https://doi.org/10.1017/S0022377821000027 Published online by Cambridge University Press

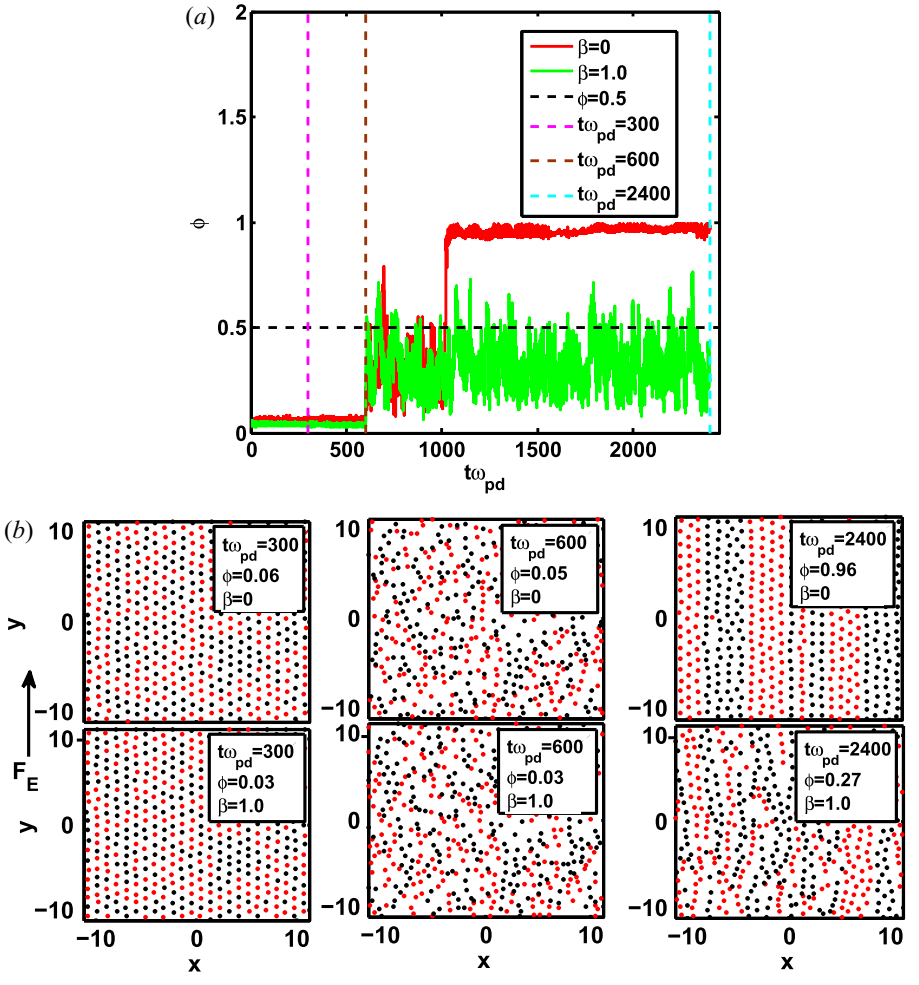

FIGURE 9. Lane formation dynamics both in the presence and absence of the external magnetic field for the constant electric field case. (*a*) Order parameter ϕ versus $t\omega_{\rm pd}$ plot for the constant field case, both in the presence ($\beta = 1.0$) and absence ($\beta = 0.0$) of the external magnetic field. Here, electric field is applied at $t\omega_{\rm pd} = 600$ time step. The vertical dashed lines indicate the time at which the simulation snapshots are collected and plotted as shown in figure 9(*b*). The other parameters used are $E_0 = 150$, $\Gamma = 14.1$ and $\rho = 1.0$. (*b*) Typical simulation snapshots taken at $t\omega_{\rm pd} = 300$, 600, 2400, showing lane formation dynamics in the constant electric field case, both in the presence ($\beta = 1.0$) and absence ($\beta = 0.0$) of the external magnetic field. The other parameters used are $E_0 = 150$, $\Gamma = 14.1$ and $\rho = 1.0$.

4.1.2. *Oscillatory field*

In this subsection, the lane formation dynamics of 2-D PIP in the presence of an external oscillating electric field ($\omega \neq 0$) by simulating Langevin molecular dynamics is presented. In particular, we have examined the effect of external magnetic field ($\beta \neq 0$) on lane formation. Here, the external magnetic field is applied from the beginning of the simulation, and external electric field is applied from $t\omega_{\rm pd} = 600$ time step in the case under study.

https://doi.org/10.1017/S0022377821000027 Published online by Cambridge University Press

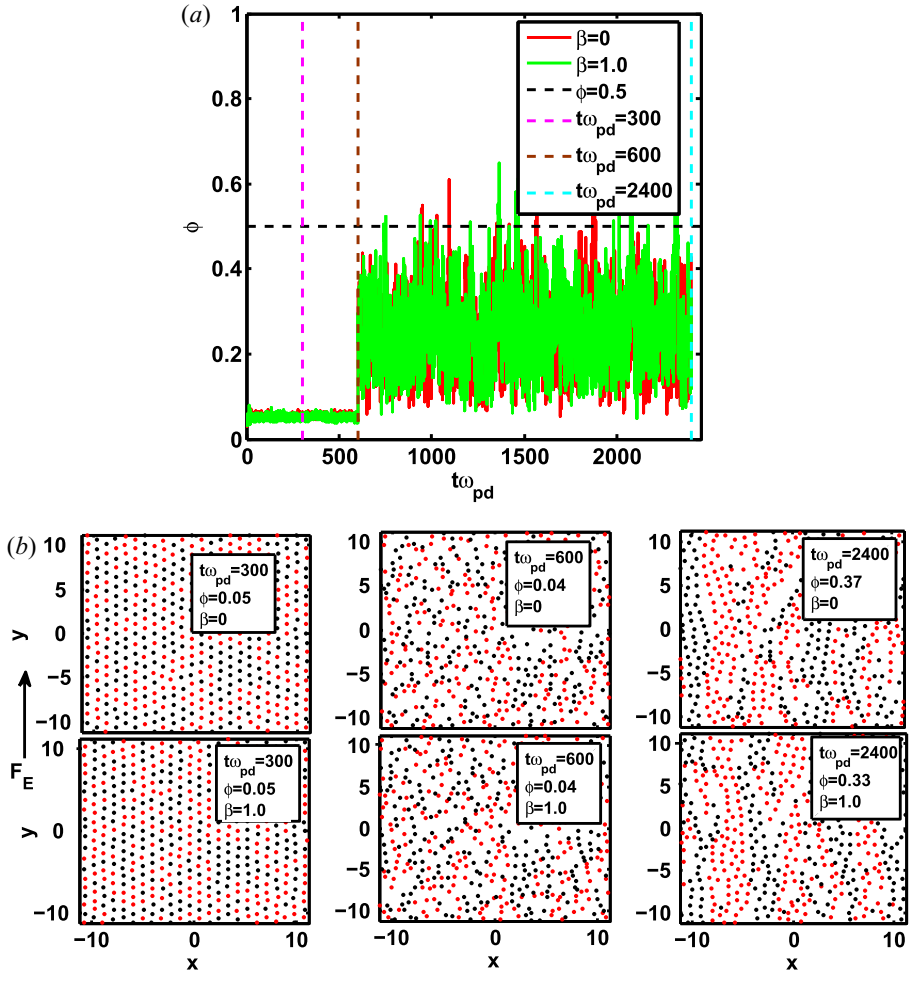

FIGURE 10. Lane formation dynamics both in the presence and absence of the external magnetic field for constant electric field case. (*a*) Order parameter ϕ versus $t\omega_{\rm pd}$ plot for constant field case, both in the presence ($\beta = 1.0$) and absence ($\beta = 0.0$) of the external magnetic field. Here, electric field is applied at $t\omega_{\rm pd} = 600$ time step. The vertical dashed lines indicate the time at which the simulation snapshots are collected and plotted as shown in figure 10(*b*). The other parameters used are $E_0 = 150$, $\Gamma = 15.0$ and $\rho = 1.0$. (*b*) Typical simulation snapshots taken at $t\omega_{\rm pd} = 300$, 600, 2400, showing lane formation dynamics in the constant electric field case, both in the presence ($\beta = 1.0$) and absence ($\beta = 0.0$) of the external magnetic field. The other parameters used are $E_0 = 150$, $\Gamma = 15.0$ and $\rho = 1.0$.

In this subsection, in figure 13(*a*), the simulation snapshots associated with a situation are plotted at different simulation times for an external electric field having sinusoidal oscillation and of strength $E_0 = 150$, frequency $\omega = 0.001$, $\Gamma = 2.6$, $\rho = 0.5$ and in the presence of the external magnetic field with $\beta = 1.0$. The initial snapshot at $t\omega_{\rm pd} = 300$ with $\phi = 0.037$ corresponds a disordered phase. This snapshot is taken just before the external electric field is switched on at $t\omega_{\rm pd} = 600$. The second snapshot is taken at $\omega = 910$ having $\phi = 0.71$, when the system reaches to a lane formation state. The next snapshot is taken at $t\omega_{\rm pd} = 1634$ with $\phi = 0.125$ showing the disordered state and at $t\omega_{\rm pd} = 2242$,

https://doi.org/10.1017/S0022377821000027 Published online by Cambridge University Press

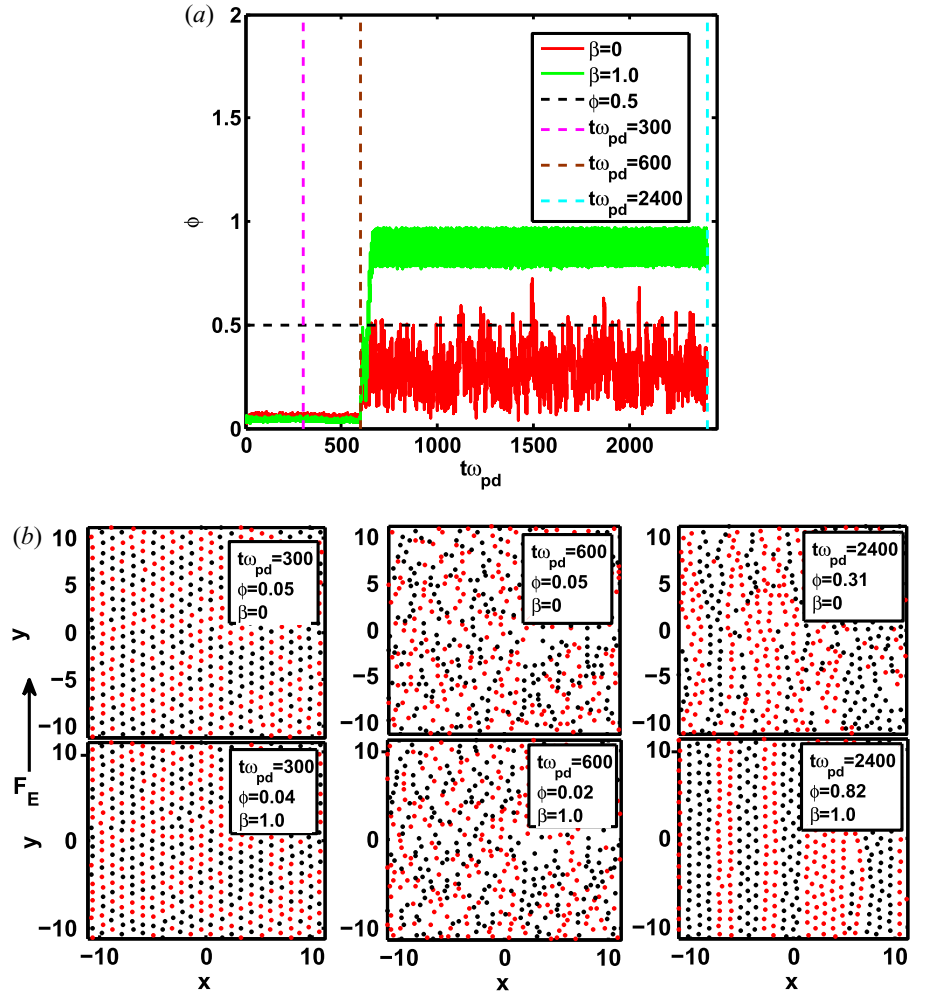

FIGURE 11. Lane formation dynamics both in the presence and absence of the external magnetic field for the constant electric field case. (*a*) Order parameter ϕ versus $t\omega_{\rm pd}$ plot for the constant field case, both in the presence ($\beta = 1.0$) and absence ($\beta = 0.0$) of the external magnetic field. Here, electric field is applied at $t\omega_{\rm pd} = 600$ time step. The vertical dash lines indicate the time at which the simulation snapshots are collected and plotted as shown in figure 11(*b*) below. The other parameters used are $E_0 = 150$, $\Gamma = 14.2$ (phase transition location, see figure 6*a*) and $\rho = 1.0$. (*b*) Typical simulation snapshots taken at $t\omega_{\rm pd} = 300$, 600, 2400, showing lane formation dynamics in the constant electric field case, both in the presence ($\beta = 1.0$) and absence ($\beta = 0.0$) of the external magnetic field. The other parameters used are $E_0 = 150$, $\Gamma = 14.2$ and $\rho = 1.0$.

the system again reaches to ordered lane state with $\phi = 0.791$, as shown in the last snapshot of figure 13(*a*). This whole process of spontaneous formation and breaking of lane structures is observed to repeat during our extensive long-time simulations in the presence of external magnetic field in the lower electric frequency range, like in our previous study in the absence of the external magnetic field[6]. This result is also supported by the time variation of the lane order parameter plot as shown in figure 13(*b*). From figure 13(*b*), it is also observed that for the frequency $\omega = 0.001$, the order parameter

https://doi.org/10.1017/S0022377821000027 Published online by Cambridge University Press

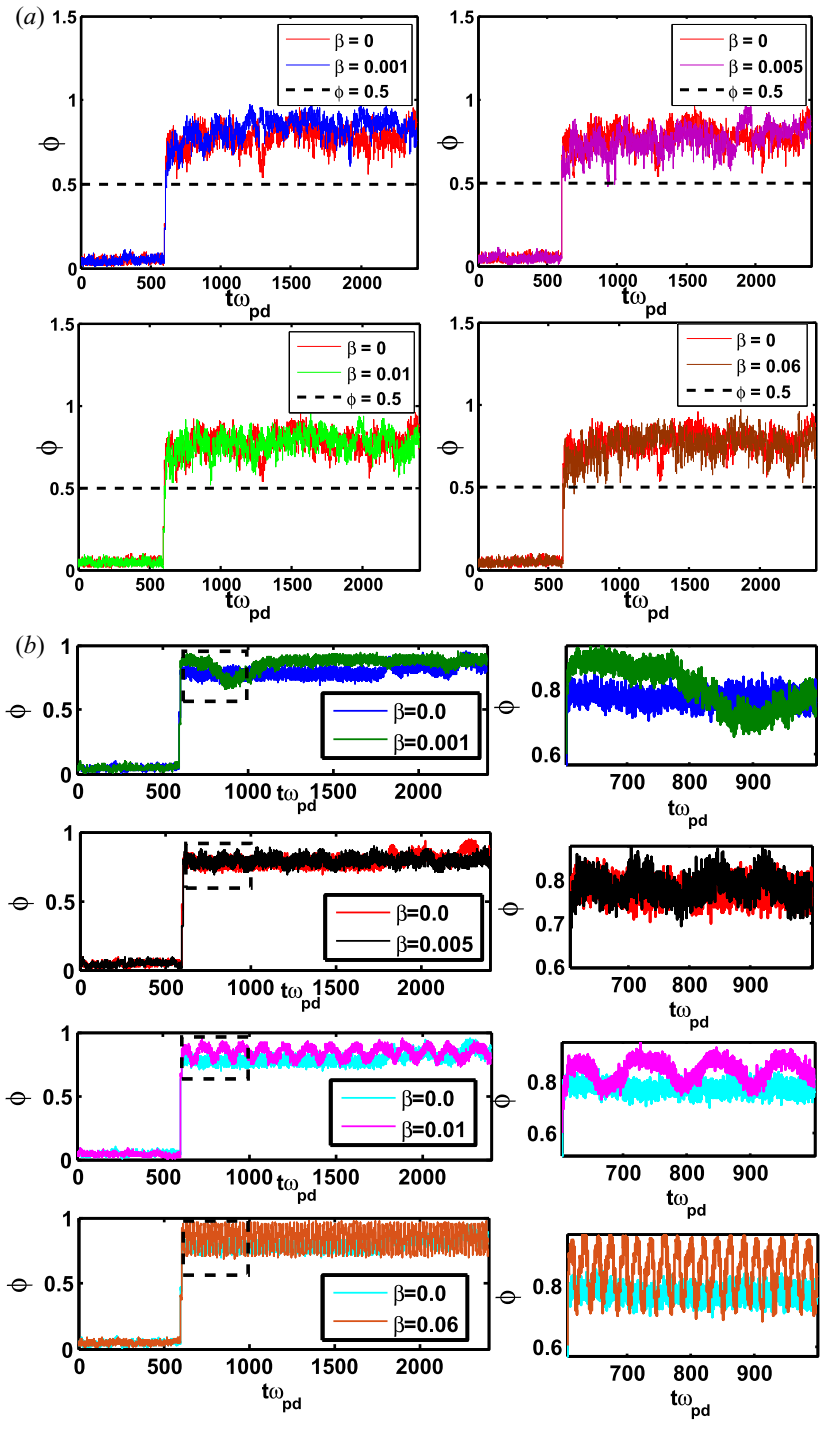

FIGURE 12. For caption see on next page.

https://doi.org/10.1017/S0022377821000027 Published online by Cambridge University Press

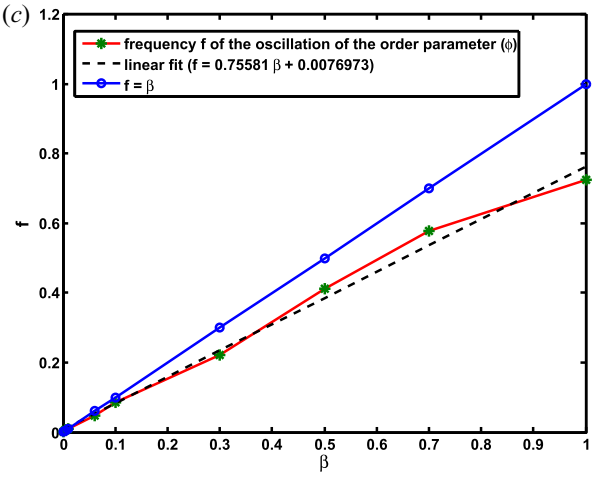

FIGURE 12. (cntd.) (*a*) Variation of order parameter (ϕ) versus $t\omega_{\rm pd}$ for varying magnetic field strength $\beta = 0.001, 0.005, 0.01, 0.06$ compared with that of $\beta = 0$ case taking $\Gamma = 2.5$. The other parameters used are $E_0 = 150$, $\rho = 1.0$, $\omega = 0.0$. (*b*) Variation of order parameter (ϕ) versus $t\omega_{\rm pd}$ for varying magnetic field strength $\beta = 0.001, 0.005, 0.01, 0.06$ compared with that of $\beta = 0$ case taking $\Gamma = 5.0$. The figures in the second column are zoomed plots from $t\omega_{\rm pd} = 600$ to 1000. The other parameters used are $E_0 = 150$, $\rho = 1.0$, $\omega = 0.0$. (*c*) The β dependence of the frequency of oscillation (f) of the order parameter (ϕ); the dashed black line is the linear fitting and the blue solid line locates $f = \beta$. The other parameters used are $\Gamma = 5.0$, $E_0 = 150$, $\rho = 1.0$, $\omega = 0.0$.

(ϕ) value decreases beyond the critical value of $\phi = 0.5$ at some points of simulation, which indicates that the system has a tendency to transit from an ordered lane state to a disordered mixed phase. The lane structure (with $\phi \approx 1$) formed at some special moments breaks up spontaneously, but the resulting disorganized state ($\phi \approx 0$) is unstable, and the lane formation immediately proceeds again, resulting in the spikes of ϕ in figure 13(*b*). This phase transition observed here in figure 13(*a*,*b*) in the presence of the oscillatory external electric field and uniform external magnetic field can be understood in the following way. In the segregated mixture, the PIP particles are moving collectively with the external electric field. Due to the oscillatory external electric field the velocity of the particles in field direction changes sign but roughly has the modulus of the ideal drift velocity. At the interfaces between two lanes, there is an additional friction due to the oppositely moving particles of the other type. Hence, the drift velocity near an interface changes sign periodically according to the shaking external field. Now, for the stability of two lanes at their interface, the field frequency (ω) has to be small enough in order to provide a sufficiently long time period in which the two lanes can slide against each other avoiding a mixing of different particle species, and lanes are not destroyed. If this time is getting small, diffusion perpendicular to the field direction will dominate and destroy the sharp interface, and this can be observed from figure 13(*c*) where time variation of ϕ is plotted for larger, intermediate and lower frequency values. From figure 13(*c*), it is also observed that ϕ oscillation tends to disappear for the intermediate frequency value ($\omega = 0.7$) before the plasma loses its self-organization for the larger frequency value ($\omega = 7.0$). For intermediate frequency values ($\omega = 0.7$), the particles get comparatively less chance for interaction with different kind of particles, this restrains effectively the random motion of the particles, as a result, the particles are not likely to get entangled into

https://doi.org/10.1017/S0022377821000027 Published online by Cambridge University Press

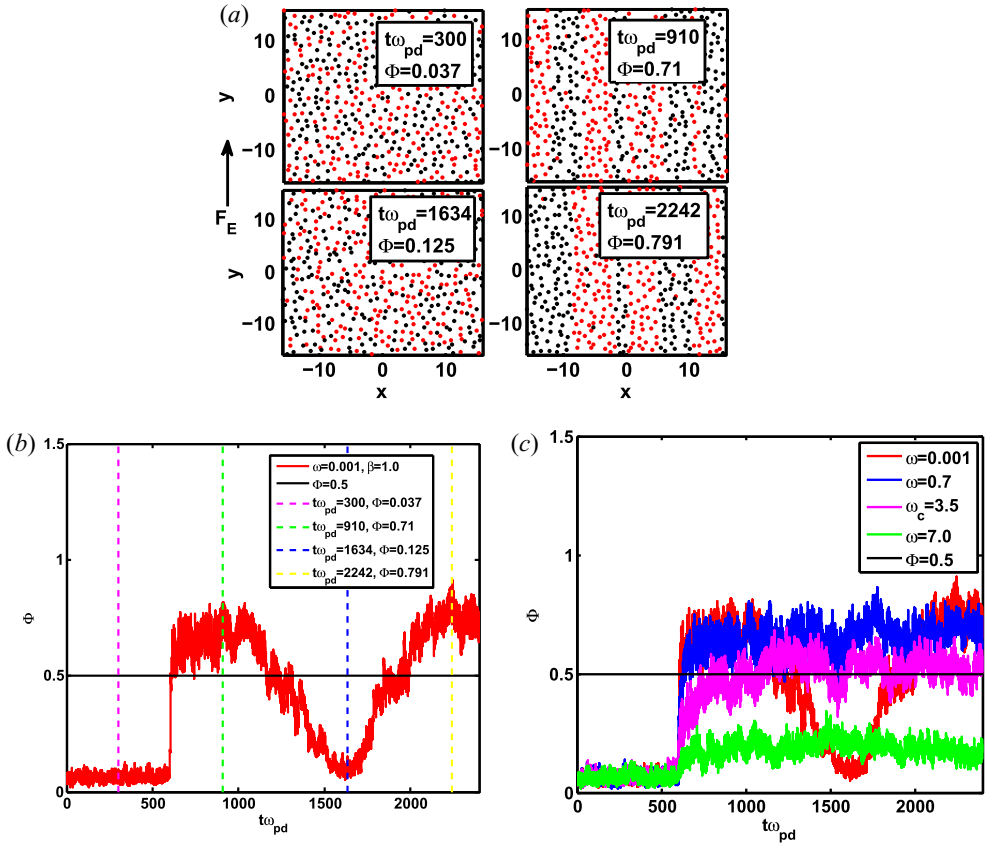

FIGURE 13. Lane formation dynamics in the presence of the external magnetic field (with $\beta = 1.0$) for oscillatory electric field case ($\omega \neq 0$). (*a*) Typical simulation snapshots taken at $t\omega_{\rm pd} = 300$, 910, 1634, 2242, showing spontaneous lane formation and deformation dynamics in the oscillatory electric field case ($\omega = 0.001$), in the presence of external magnetic field ($\beta = 1.0$). The other parameters used are $E_0 = 150$, $\Gamma = 2.5$, $\rho = 0.5$. (*b*) Time variation of order parameter (ϕ) plot taking the external oscillatory electric field frequency $\omega = 0.001$ in the presence of external magnetic field ($\beta = 1.0$). The vertical dashed lines indicate the time at which instantaneous position of the PIP particles (see, figure 13*c*) are recorded. The other parameters used are $E_0 = 150$, $\Gamma = 2.5$, $\rho = 0.5$. (*c*) Time variation of order parameter (ϕ) plot for $\omega = 0.001$, 0.7, 3.5, 7.0 in the presence of external magnetic field ($\beta \neq 0$). The other parameters used are $E_0 = 150$, $\Gamma = 2.5$, $\rho = 0.5$ and $\beta = 1.0$.

another lane and lanes are not destroyed. Moreover, like the constant electric field with finite β case, here, in the oscillatory electric field with $\beta = 1.0$ case also the lanes seem to move along the X-direction of the simulation chamber, which indicates the ($E \times B$) drift effect.

As shown in figure 13(*c*), for the oscillatory external electric field case, from the order parameter ϕ versus $t\omega_{\rm pd}$ plot for various frequency values, the critical frequency ($\omega = \omega_c$) upon which a transition of the system back to the disordered state occurs can be understood, if an oscillating field with amplitude $E_0 > E_c$ is present. Like our previous study (Sarma *et al.* 2020) in the absence of the external magnetic field, here, in the presence of the external magnetic field also, it is evident from figure 13(*c*) that lane formation with the oscillating sinusoidal electric field depends on the value of ω. If an

https://doi.org/10.1017/S0022377821000027 Published online by Cambridge University Press

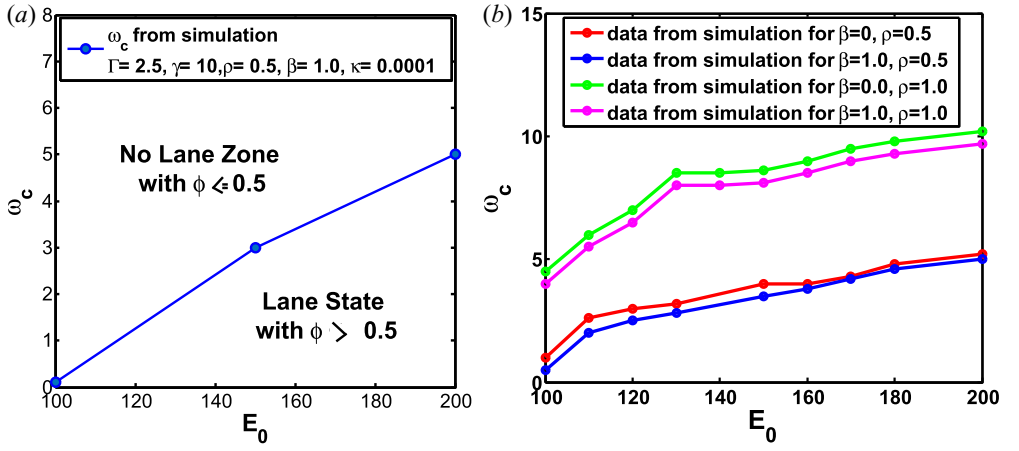

FIGURE 14. Non-equilibrium phase diagram for 2-D PIP system with oscillatory external electric field in the application of the external magnetic field. (*a*) Non-equilibrium phase diagram with oscillatory external electric field ($\omega \neq 0$) in the presence of the external magnetic field ($\beta = 1.0$) showing lane zone and disordered zone. The other parameters used are $\Gamma = 2.5$, $\rho = 0.5$. (*b*) Non-equilibrium phase diagram with oscillatory external electric field ($\omega \neq 0$), both in the presence ($\beta = 1.0$) and absence ($\beta = 0$) of the external magnetic field for different ρ values. The other parameters used are $\Gamma = 2.5$, $E_0 = 2.5$.

oscillating field with amplitude $E_0 > E_c$ is present and the frequency ω is increased, the order parameter ϕ decreases with increasing ω. For low frequencies the system remains in the lane state, while above a critical frequency (ω_c), the system goes back to the disordered state. In the present case, $\omega_c = 3.5$ where $\phi \approx 0.5$. Above $\omega_c = 3.5$ the system remains in the disordered state with $\phi < 0.5$ as shown in figure 13(*c*). With this concept, the phase diagram for an underdamped PIP system with an oscillating sinusoidal external electric field and in the presence of an external uniform magnetic field taking density $\rho = 1.0$ is plotted and is shown in figure 14(*a*). The same is plotted in figure 14(*b*) for different values of densities ($\rho = 0.5, 1.0$) taking into consideration both the presence ($\beta = 1.0$) and absence ($\beta = 0.0$) of the external magnetic field. In both the cases (figure 14*a*,*b*), the critical external oscillating field frequency ω_c is plotted versus E_0. The trend of the ω_c increases with increasing E_0, as can be seen in both figures 14(*a*) and 14(*b*). From figure 14(*b*), it is also observed that the trend of ω_c increases with increasing density ρ. In figure 14(*b*), the ω_c values obtained in the absence of the external magnetic field ($\beta = 0.0$), for density values $\rho = 0.5, 1.0$, are plotted along with the results obtained in the presence of the external magnetic field $\beta \neq 0.0$, and clearly it is observed that upon application of magnetic field, a lower value of critical field frequency is required to transit the system from the ordered lane state to the disordered state.

In figure 15, time variation of the order parameter ϕ is plotted for different values of magnetic field, ranging from $\beta = 0.0$ to $\beta = 1.0$ (although few are plotted here) taking input parameters as $E_0 = 150$, $\omega = 0.001$, $\Gamma = 2.5$ and $\rho = 1.0$. The figure shows that the varying magnetic field strength does not bring any significant change in the trend of order parameter ϕ with time for a lower $\Gamma = 2.5$ value. This can also be understood from comparative time variation of order parameter plots both in the presence and absence of the external magnetic field, as shown in figure 16(*a*). Here, the input parameters are the same as used in the case of figure 15. In figure 16(*b*), a similar type of time variation of order parameter data are plotted, but, taking $\Gamma = 5.0$, and it is observed that with an

https://doi.org/10.1017/S0022377821000027 Published online by Cambridge University Press

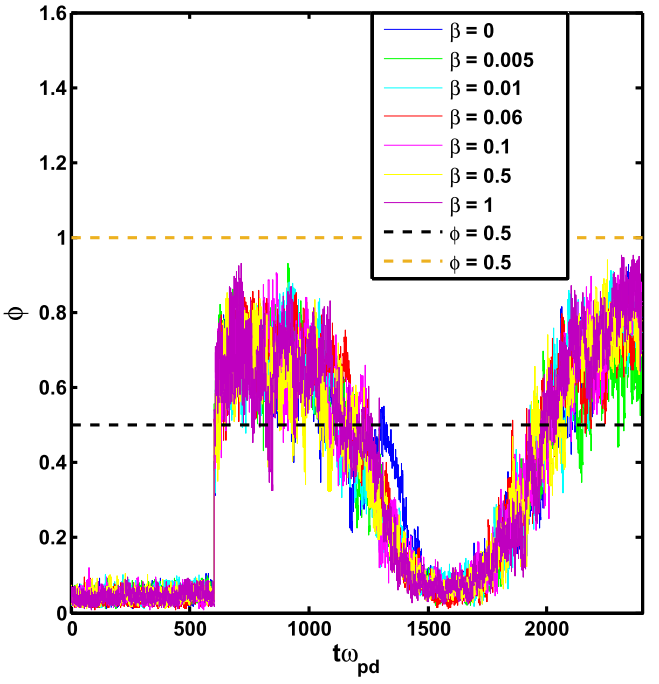

FIGURE 15. Time variation of order parameter (ϕ) plot for various values of the external magnetic field strength $\beta = 0, 0.005, 0.01, 0.06, 0.1, 0.5, 1.0$, in the presence of the oscillatory ($\omega \neq 0$) external electric field having strength $E_0 = 150$. The other parameters used are $\Gamma = 2.5$, $\rho = 1.0$.

increase in β value, an oscillatory pattern of the order parameter plots appears and the frequency of corresponding oscillation increases with an increase in β value. This is seen for the whole range of magnetic field strength under study for $\Gamma = 5.0$.

For an oscillating external electric field case, to study the effect of external magnetic field on critical frequencies (ω_c), data for the ω_c are also plotted versus β, as shown in figure 17. The study is performed by taking a range of β values starting from $\beta = 0.001, 0.005$ to $\beta = 1.0$, along with considering the case where external magnetic field is absent ($\beta = 0.0$), taking $E_0 = 150$, $\Gamma = 2.5$ and $\rho = 1.0$. The critical frequency ω_c is obtained by setting $\phi = 0.5$, for the set of runs with increasing frequency ω, corresponding to all the values of β. As can be identified from the figure, the ω_c value corresponding to $\beta = 0.0$ is 7.7, however, for $\beta = 0.001, 0.005$, the corresponding ω_c values are obtained as $w_c = 7.6, 7.0$, respectively. It is observed that for a further increase in β values to $\beta = 0.007$, the ω_c value decreases further to 6.5. However, from $\beta = 0.01$, it starts to increase gradually and for the rest of the higher β values it maintains the same pattern and finally, as can be seen, for $\beta = 1.0$, ω_c is obtained as 8.1. Here, one sees that a critical value of the electric field frequency below which self-organization takes place also exists and the critical frequency is an increasing function of higher β values.

4.2. *Lane formation in the presence of oblique electric field*

In this section, we have presented the lane formation dynamics of PIP by choosing the external electric force to be operative in an oblique way by making an angle θ with the X–Y plane of the simulation box. The study is performed both in the presence and absence

https://doi.org/10.1017/S0022377821000027 Published online by Cambridge University Press

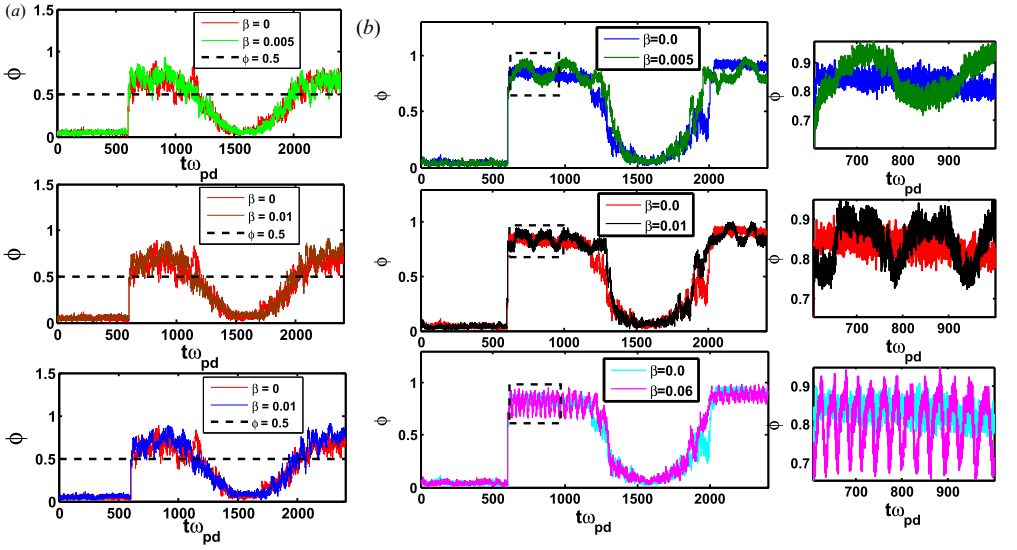

FIGURE 16. Comparative time variation of order parameter (ϕ) plot for two different values of Coulomb coupling parameter ($\Gamma = 2.5, 5.0$), both in the absence ($\beta = 0$) and presence ($\beta \neq 0$) of the external magnetic field. (a) Time variation of order parameter (ϕ) plot for the external magnetic field strength values $\beta = 0$, 0.005, 0.01, 0.06, for a PIP system in the presence of the oscillatory external electric field having frequency ($\omega = 0.001$). The Coulomb coupling parameter value used here is $\Gamma = 2.5$; the other parameters used are $E_0 = 150$, $\rho = 1.0$. (b) Time variation of order parameter (ϕ) plot for the external magnetic field strength values $\beta = 0$, 0.005, 0.01, 0.06, for a PIP system in the presence of the oscillatory external electric field having frequency ($\omega = 0.001$). The figures in the second column are zoomed plots from $t\omega_{\rm pd} = 600$ to 1000. The plots are showing an oscillatory pattern of ϕ, which increases with increasing β, for clarity, zoomed plots are mentioned on the right-hand side. The parameters used are $\Gamma = 5.0$, $E_0 = 150$, $\rho = 1.0$.

of the external magnetic field. In particular, we have examined the effect of the external magnetic field on lane formation. The effect of system asymmetry on lane formation has also been studied here.

4.2.1. *Symmetric system*

In this subsection, the whole study has been performed by using a regular square shaped simulation chamber ($X = Y = L$, a symmetric system). Here, first, we will discuss the results obtained from a study performed for a constant electric field ($\omega = 0$) case which is applied obliquely for various values of θ, in the presence ($\beta = 1.0$) of the external magnetic field. Second, the results obtained from the obliquely applied oscillatory electric field case ($\omega \neq 0, \theta \neq 0$), in the presence of the external magnetic field have also been discussed. For both the above mentioned cases, a comparative study on lane formation dynamics is performed both in the presence and absence of the external magnetic field and results are mentioned below.

In figure 18, the instantaneous positions of the particles are plotted at different values of θ, ranging from $\theta = 30^\circ, 45^\circ$ to $\theta = 225^\circ$ taking constant electric field case with $\beta = 1.0$. The other parameters used are $E_0 = 170$, $\omega = 0$, $\Gamma = 2.5$ and $\rho = 1.0$. In this case, the forcing due to the oblique electric field is presented throughout the simulation duration after $t\omega_{\rm pd} = 600$ time steps. In figure 18, from the snapshot obtained for $\beta = 1.0$, $\theta = 30^\circ$,

https://doi.org/10.1017/S0022377821000027 Published online by Cambridge University Press

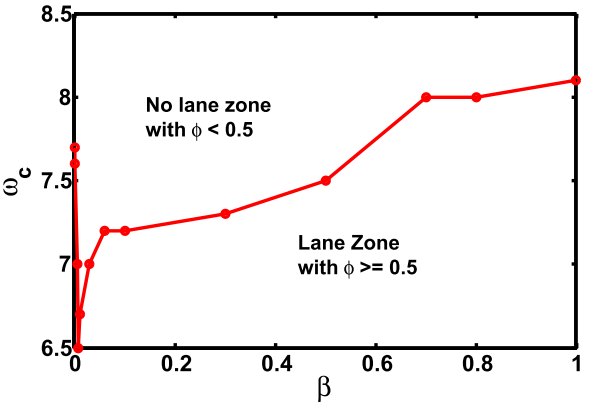

FIGURE 17. Variation of the critical value of the electric field frequency (ω_c) with β plot. Input parameters used are $E_0 = 150$, $\Gamma = 2.5$, $\rho = 1.0$, $\Delta t = 0.003$.

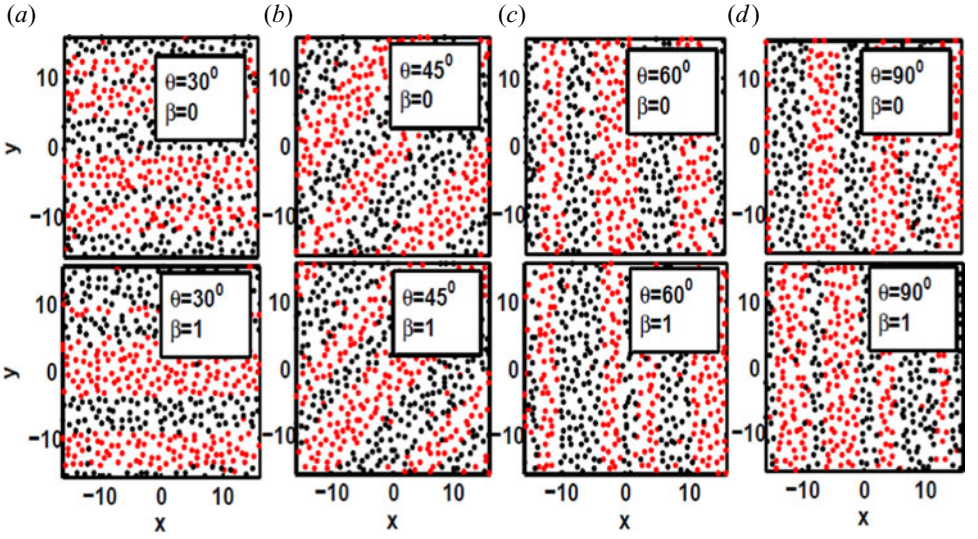

FIGURE 18. Instantaneous position of particles in the application of constant ($\omega = 0$) oblique electric field taking $\theta = 30^\circ, 45^\circ, 60^\circ, 90^\circ$ (θ is the angle made by the electric field with the x-direction), external electric force $\boldsymbol{F}_E$ acting on the particles pointing in the Y-direction; other parameters used are $E_0 = 170$, $\Gamma = 2.5$, $\rho = 1.0$. This study is performed both in the presence ($\beta = 1$) and absence ($\beta = 0$) of the external magnetic field.

one can clearly observe lane structures where the direction of the lanes coincides with the X-axis of the simulation box. For $\theta = 45^\circ$ with $\beta = 1.0$, some steady lane states are observed with tilted bands, see the snapshot in figure 18. These tilted lanes seen in the simulations might be artefacts of the external electric field used obliquely ($\theta = 45^\circ$) in the simulation. With further increasing the oblique angle to $\theta = 60^\circ$, lane formation occurs where the direction of the lanes coincides with the Y-direction of the simulation chamber. Lastly with $\theta = 90^\circ$, the typical lane structures are formed parallel to the drive direction, see the corresponding snapshot in figure 18. To verify whether the tilted bands that are observed for $\theta = 45^\circ$ (figure 18) will be reformed, several simulations are performed for different θ values, and for $\theta = 135^\circ$ and 225°, reappearance of the similar kind of tilted

https://doi.org/10.1017/S0022377821000027 Published online by Cambridge University Press

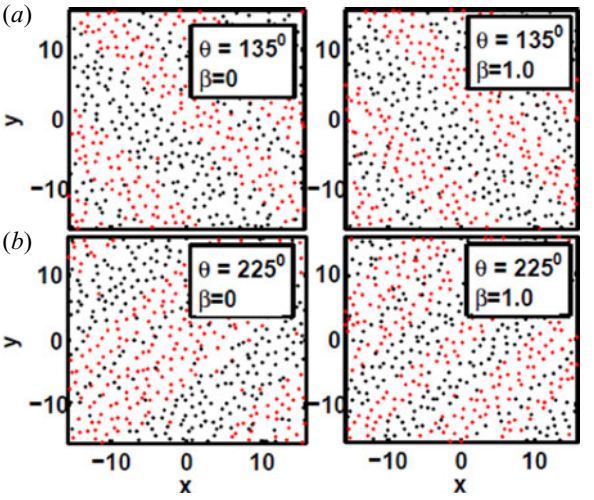

FIGURE 19. Instantaneous position of particles in the application of constant ($\omega = 0$) oblique electric field taking $\theta = 135^\circ, 225^\circ$ (θ is the angle made by the electric field with x-direction), external electric force $\boldsymbol{F}_E$ acting on the particles pointing in the Y-direction; other parameters used are $E_0 = 170$, $\Gamma = 2.5$, $\rho = 1.0$. This study is performed both in the presence ($\beta = 1$) and absence ($\beta = 0$) of the external magnetic field.

bands are observed for both in the presence and absence of the external magnetic field, the related particle snapshots for the constant electric field case are plotted, as shown in figure 19.

From our study similar types of pattern formations are also observed in the case of the oscillatory electric field having frequency of oscillation $\omega = 2.0$, applied obliquely making the same magnitude of the oblique angles ($\theta = 30^\circ, 45^\circ, 60^\circ, 90^\circ$) with the X–Y plane of the simulation box as used in the constant field case, in the presence of the external magnetic field. The related particle snapshots are plotted as shown in figure 20. The other parameters used for this study are $E_0 = 170$, $\Gamma = 2.5$ and $\rho = 1.0$. From our study, a similar trend of the lane structures is also observed in the absence of the external magnetic field ($\beta = 0$), as it is obtained in the presence of both the obliquely applied constant (see figure 18 for the $\omega = 0$ case) and oscillatory electric fields (see figure 19 for the $\omega \neq 0$ case). The only difference observed between the results obtained from the oblique force field cases in the presence and absence of the external magnetic field is that, in the presence of the external magnetic field ($\beta = 1.0$), the movement of the lanes is observed in the plane (X–Y) perpendicular to the direction of the applied external magnetic field (Z-direction), which is not observed in the absence of the magnetic field. This movement of the lanes in the X–Y plane in the presence of the external magnetic field indicates the presence of the ($E \times B$) drift in the system.

4.2.2. *Asymmetric system*

In this subsection, the whole study has been performed by using an asymmetric simulation chamber, $X = 20Y$, to observe the effect of the aspect ratio on lane formation dynamics. The aspect ratio is a fundamental quantity that denotes the proportional ratio between the individual system sizes. We find that the lane formation does not depend on either X or Y separately (X, Y represent system lengths), rather, the aspect ratio X/Y appears to be important. In this study, both constant ($\omega = 0$) and oscillatory ($\omega \neq 0$)

https://doi.org/10.1017/S0022377821000027 Published online by Cambridge University Press

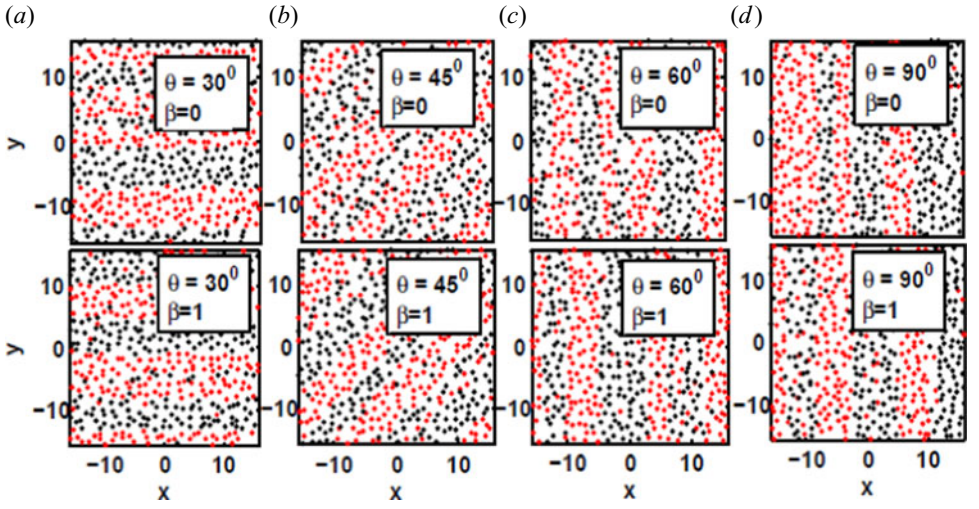

FIGURE 20. Instantaneous position of particles in the application of oscillatory ($\omega \neq 0$) oblique electric field taking $\theta = 30^\circ, 45^\circ, 60^\circ, 90^\circ$ (θ is the angle made by the electric field with x-direction), external electric force $\boldsymbol{F}_E$ acting on the particles pointing in the Y-direction; other parameters used are $E_0 = 170$, $\omega = 2.0$, $\Gamma = 2.5$, $\rho = 1.0$. This study is performed both in the presence ($\beta = 1$) and absence ($\beta = 0$) of the external magnetic field.

electric fields are used, which are applied obliquely for various values of θ. To see the effect of external magnetic field, here a comparative studies has also been performed both in the presence and absence of the magnetic field.

In figure 21, instantaneous particle positions are plotted for $\theta = 30^\circ$, 45°, 60° and 90°, keeping all the other input parameters values as same as used in the case of the symmetric system in the presence of the constant electric field (see, figure 18). This present study reveals that lane formation is observed for $\theta = 30^\circ$ only, using an asymmetric simulation chamber. There is no lane formation occurring for higher values of θ, i.e. $\theta > 30^\circ$. However, this dependence on aspect ratio is not understood theoretically. A similar lane formation trend is also observed both in the presence and absence of the external magnetic field. However, for the obliquely applied oscillatory ($\omega = 2.0$) electric field case, the lane formation observed inside the simulation chamber for the oblique angle $\theta = 60^\circ$ only, the lanes are aligned with the X-direction of the simulation chamber as shown in figure 22. The other parameters used are $E_0 = 170$, $\Gamma = 2.5$ and $\rho = 1.0$. A similar lane formation trend is also observed in the absence of the external magnetic field by taking into consideration an obliquely applied oscillatory electric field, as shown in figure 22.

5. Conclusions

We have carried out the LD simulations to study lane formation dynamics in a 2-D PIP medium in the presence of forcing due to an external electric field. More specifically, the authors focused on the effect of an external magnetic field on the self-organization effect in the zero κ (screening parameter) case, where, the 'plasma' is structured as a set of lanes that alternatively contain positive and negative ions. The study is based on a plasma model, where, the ion–ion interaction is described with a screened electrostatic potential, and the ion–neutral background interaction is described using an overall friction force characterized by a damping factor and a zero-average stochastic collisional term that enables the description of the diffusion effect. This model is used to describe the dynamics

https://doi.org/10.1017/S0022377821000027 Published online by Cambridge University Press

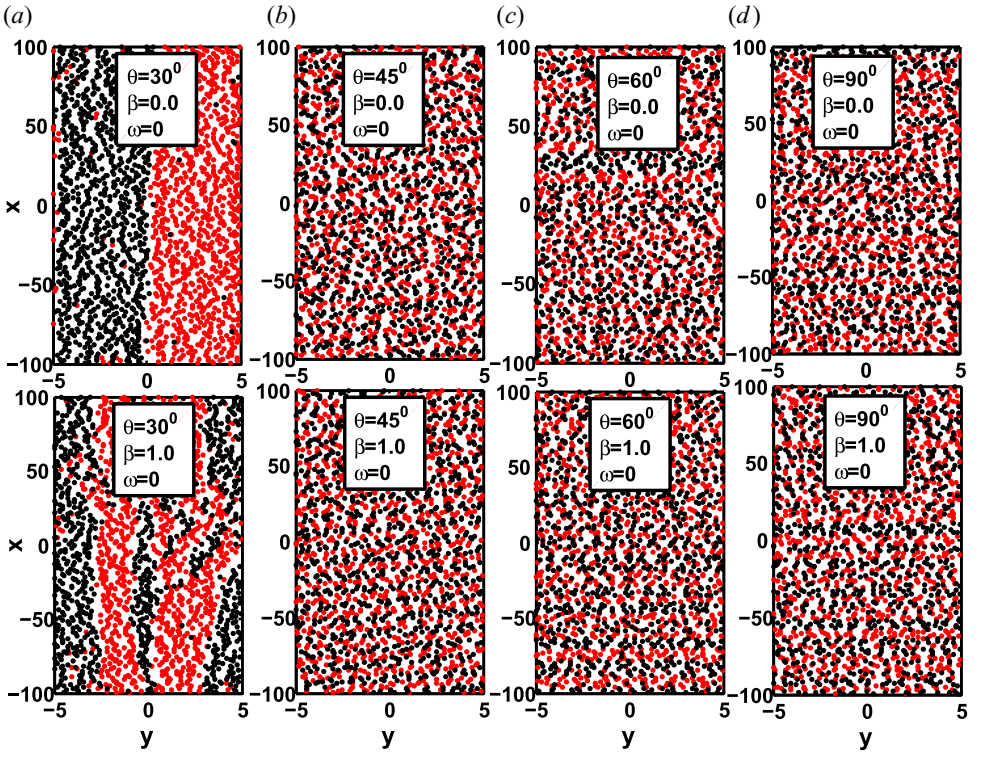

FIGURE 21. Instantaneous position of particles in the application of constant ($\omega = 0$) oblique electric field taking $\theta = 30^\circ, 45^\circ, 60^\circ, 90^\circ$ (θ is the angle made by the electric field with x-direction), external electric force $\boldsymbol{F}_E$ acting on the particles pointing in the Y-direction, an asymmetric system ($X = 20Y$) is used here; the other parameters are $E_0 = 170$, $\omega = 0.0$, $\Gamma = 2.5$, $\rho = 1.0$. This study is performed both in the presence ($\beta = 1$) and absence ($\beta = 0$) of the external magnetic field.

of a set of N ions submitted to a stationary or time-varying electric field in a 2-D domain in the presence of an external magnetic field. This effect is quantitatively characterized in terms of an order parameter ϕ. Although the dynamics of lane formation has already been reported in our earlier work (Sarma *et al.* 2020), where self-organization was investigated only in the case of an external electric field in finite κ limit. In the present work, we consider a much broader situation where the applied external magnetic field is significant and the obliquely applied external electric field is also taken into consideration along with the constant and oscillatory fields.

The paper brings new and interesting information as far as this self-organization effect is concerned in the presence of an external magnetic field. In particular, we finish with the following list of conclusions.

(i) A critical value of the electric field above which self-organization takes place exists in the presence of the external magnetic field ($\beta \neq 0$).
(ii) This critical value of the electric field strength is larger than the one obtained in the absence of the external magnetic field. The higher the magnetic field strength, the higher the strength of external electric field required to reach the transition point.
(iii) The critical value of field strength increases with an increase of the density (ρ) of the system in the presence of the external magnetic field.

https://doi.org/10.1017/S0022377821000027 Published online by Cambridge University Press

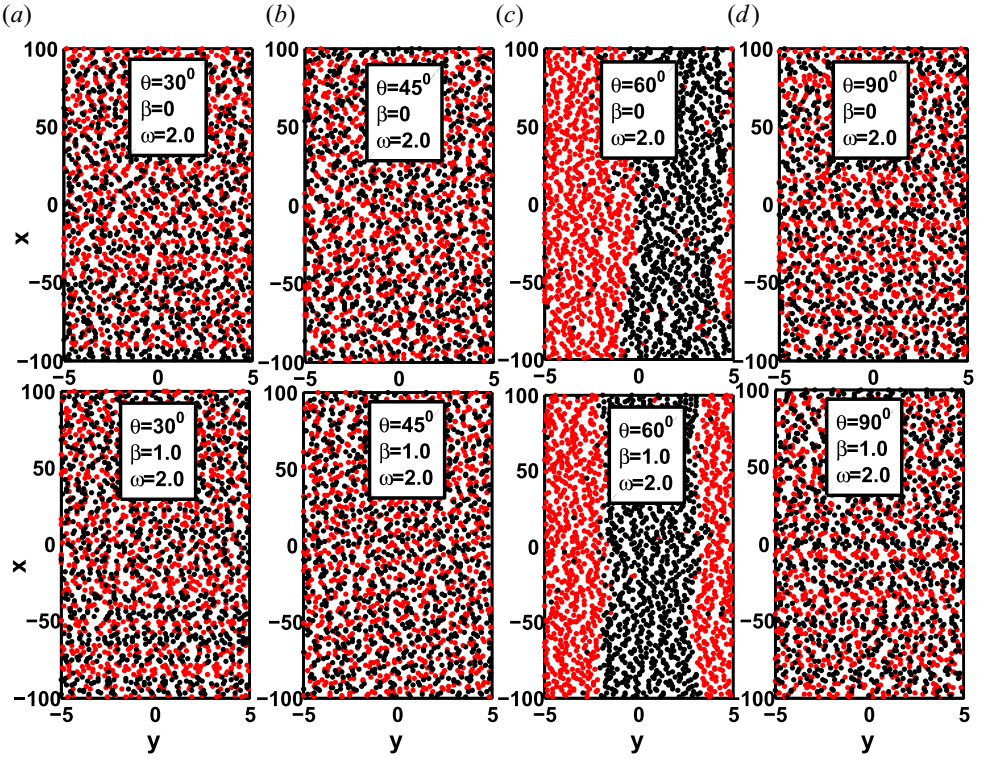

FIGURE 22. Instantaneous position of particles in the application of oscillatory ($\omega \neq 0$) oblique electric field taking $\theta = 30^\circ, 45^\circ, 60^\circ, 90^\circ$ (θ is the angle made by the electric field with x-direction), external electric force $\boldsymbol{F}_E$ acting on the particles pointing in the Y-direction, an asymmetric system ($X = 20Y$) is used here; the other parameters are $E_0 = 170$, $\omega = 2.0$, $\Gamma = 2.5$, $\rho = 1.0$. This study is performed both in the presence ($\beta = 1$) and absence ($\beta = 0$) of the external magnetic field.

(iv) Due to the presence of both uniform electric and magnetic fields, the PIP particles experience a drift of the guiding centre ($E \times B$ drift) and as a result of that, the self-organized lanes start to move along a direction perpendicular to both the directions of the applied electric and magnetic fields with a velocity $v_E = E_0/\beta$ (in MD units). It is also observed that the speed of these lane movements increases with an increase of the applied electric field strength in the presence of the uniform external magnetic field.

(v) The self-organization is correlated to a strong decrease of the transverse diffusion coefficient (D_{xL}) in the zero β case (absence of the magnetic field). Unlike the zero β case, for the finite β case, the value of D_{xL} goes on increasing along with the electric field strength E_0, which signifies the presence of the $E \times B$ drift in the system.

(vi) The phase diagram obtained from the Γ scan of the order parameter (ϕ) values, for a PIP system with constant external electric field both in the presence and absence of the external magnetic field shows a lane formation–disintegration phase. In all the cases, for the lower Γ value side, a critical Coulomb coupling parameter (Γ_{lc}) appears below which the PIP system is in a disordered phase with $\phi < 0.5$. The lane formation area extends for a wide rage of Γ values starting from Γ_{lc} before

https://doi.org/10.1017/S0022377821000027 Published online by Cambridge University Press

to disappear to a disordered phase above a critical Coulomb coupling parameter (Γ_{hc}) value in higher side of Γ. However, a further increase of the Γ value lanes reappeared again in some particular point in the presence of an external magnetic field only.

(vii) Our investigation demonstrates that due to the presence of both electric and magnetic fields, the PIP particles experience ($E \times B$) drift which occurs in the form of fluctuations in the order parameter plot in a strongly coupled regime for both the presence of constant and oscillatory external electric fields. The frequency of these fluctuations vary with varying magnitude of the magnetic field strength.

(viii) The PIP shows a non-stationary lane-like self-organization behaviour, with oscillation between self-organized and random states for the small frequency values, when submitted to a time-varying electric field in the presence of external magnetic field also. The lanes are found to move along a direction perpendicular to the both E and B field directions as a result of the guiding centre drift.

(ix) For each electric field, there exists a critical frequency ω_c, above which the system cannot reach the self-organized state.

(x) The critical frequency is an increasing function of the electric field in the presence of an external magnetic field.

(xi) Upon application of a magnetic field, a lower value of critical field frequency is required to transit the system from an ordered lane state to a disordered state.

(xii) The stability study of lanes identifies the intermediate frequency value, in the presence of the external magnetic field, where ϕ oscillation tends to disappear before the plasma loses its self-organization (for larger frequency). This intermediate frequency value in the absence of the external magnetic field is much higher than that in the presence of an external magnetic field.

Finally, the study of lane dynamics has been performed using an oblique (oblique angle $\theta \neq 0$) electric force on a PIP system both in the presence and absence of the external magnetic field for a range of oblique angles $\theta = 30^\circ \longleftrightarrow 90^\circ$. This application of oblique force reveals the following.

(i) Variation of the oblique angle θ plays a significant role for achieving the lane state. For a small oblique angle ($\theta = 30^\circ$), strikingly, the system first develops structures along the X-axis. For intermediate oblique angles, i.e. for $\theta = 45^\circ$, 60°, respectively, segregated stripes of PIP particles tilted or oriented perpendicular to the X-direction of the simulation chamber. On the other hand, for $\theta = 90^\circ$, lanes are formed parallel to the direction of the electric field.

(ii) The only difference observed in this study in the presence of the external magnetic field is that, in the presence of the B field, movement of the lanes appears in a direction perpendicular to both the directions of the E and B fields. This effect is due to the presence of the electric field drift, which is not observed in the absence of the B field.

(iii) Lastly, the system aspect ratio X/Y plays a major role on the lane formation dynamics in the presence of an oblique electric field.

A study of self-organized lane structures for PIP system using LD simulation in the presence of the external magnetic field is reported here. Our simulation results may help to identify and extend the parameter range and precise location of lane formation phase in a 2-D PIP system in the presence of the external magnetic field.

https://doi.org/10.1017/S0022377821000027 Published online by Cambridge University Press

Acknowledgements

This research work is supported by the Board of Research in Nuclear Sciences (BRNS), DAE, project sanctioned no. 39/14/25/2016-BRNS/34428, date 20/01/2017; revalidation no. 39/14/25/2016-BRNS/34014, date 03/04/2017. S.B. and U.S. would like to acknowledge the Institute for Plasma Research (IPR), Bhat, Gandhinagar, for allowing us to use the HPC cluster at IPR.

Editor Roger Blandford thanks the referees for their advice in evaluating this article.

Declaration of interests

The authors report no conflict of interest.

REFERENCES

2001 Cumulative subject index. In *Cumulative Author, Title and Subject Index Including Table of Contents, Volumes 1–19* (ed. C. Domb & J. L. Lebowitz), Phase Transitions and Critical Phenomena, vol. 20, pp. 41–201. Academic Press.

AERTSENS, M. & NAUDTS, J. 1991 Field-induced percolation in a polarized lattice gas. *J. Stat. Phys.* **62** (3–4), 609–630.

ALLEN, M., ALLEN, M., TILDESLEY, D., ALLEN, T. & TILDESLEY, D. 1989 *Computer Simulation of Liquids*. Clarendon Press.

AMMELT, E., SCHWENG, D. & PURWINS, H.-G. 1993 Spatio-temporal pattern formation in a lateral high-frequency glow discharge system. *Phys. Lett.* A **179** (4), 348–354.

ARANSON, I. S. & TSIMRING, L. S. 2006 Patterns and collective behavior in granular media: theoretical concepts. *Rev. Mod. Phys*. **78**, 641–692.

ASSEO, E. 2003 Pair plasma in pulsar magnetospheres. *Plasma Phys. Control. Fusion* **45** (6), 853–867.

ASTROV, Y. A., MÜLLER, I., AMMELT, E. & PURWINS, H.-G. 1998 Zigzag destabilized spirals and targets. *Phys. Rev. Lett*. **80**, 5341–5344.

BARUAH, S. & DAS, N. 2010 The effect of magnetic field on the structure of Coulomb crystal in dusty plasma. *Phys. Plasmas* **17** (7), 073702.

BARUAH, S., GANESH, R. & AVINASH, K. 2015 A molecular dynamics study of phase transition in strongly coupled pair-ion plasmas. *Phys. Plasmas* **22** (8), 082116.

BEGELMAN, M. C., BLANDFORD, R. D. & REES, M. J. 1984 Theory of extragalactic radio sources. *Rev. Mod. Phys*. **56**, 255–351.

BERMAN, R. H., TETREAULT, D. J. & DUPREE, T. H. 1985 Simulation of phase space hole growth and the development of intermittent plasma turbulence. *Phys. Fluids* **28** (1), 155–176.

BREAZEAL, W., FLYNN, K. M. & GWINN, E. G. 1995 Static and dynamic two-dimensional patterns in self-extinguishing discharge avalanches. *Phys. Rev.* E **52**, 1503–1515.

CROSS, M. C. & HOHENBERG, P. C. 1993 Pattern formation outside of equilibrium. *Rev. Mod. Phys*. **65**, 851–1112.

DZUBIELLA, J., HOFFMANN, G. P. & LÖWEN, H. 2002 Lane formation in colloidal mixtures driven by an external field. *Phys. Rev.* E **65**, 021402.

FELICIANI, C., MURAKAMI, H. & NISHINARI, K. 2018 A universal function for capacity of bidirectional pedestrian streams: filling the gaps in the literature. *PLoS One* **13**, e0208496.

HANSEN, J.-P. & MCDONALD, I. R. 1986 *Theory of Simple Liquids*, 2nd edn. Academic Press.

HELBING, D., FARKAS, I. J. & VICSEK, T. 2000 Freezing by heating in a driven mesoscopic system. *Phys. Rev. Lett*. **84**, 1240–1243.

IKEDA, K. & KIM, K. 2017 Lane formation dynamics of oppositely self-driven binary particles: effects of density and finite system size. *J. Phys. Soc. Japan* **86** (4), 044004.

IKEDA, M., WADA, H. & HAYAKAWA, H. 2012 Instabilities and turbulence-like dynamics in an oppositely driven binary particle mixture. *Europhys. Lett*. **99** (6), 68005.

IWAMOTO, N. 1993 Collective modes in nonrelativistic electron-positron plasmas. *Phys. Rev.* E **47**, 604–611.

KANAKASABAPATHY, S. K. & OVERZET, L. J. 1998 A coupled two-sheath simulation of RF bias at high electronegativities. *Plasma Sources Sci. Technol*. **7** (3), 289–297.

KATZ, S., LEBOWITZ, J. L. & SPOHN, H. 1983 Phase transitions in stationary nonequilibrium states of model lattice systems. *Phys. Rev.* B **28**, 1655–1658.

KLYMKO, K., GEISSLER, P. L. & WHITELAM, S. 2016 Microscopic origin and macroscopic implications of lane formation in mixtures of oppositely driven particles. *Phys. Rev.* E **94**, 022608.

KOGLER, F. & KLAPP, S. 2015 Lane formation in a system of dipolar microswimmers. *Europhys. Lett*. **110**, 1–16.

KONOPKA, U., SAMSONOV, D., IVLEV, A. V., GOREE, J., STEINBERG, V. & MORFILL, G. E. 2000 Rigid and differential plasma crystal rotation induced by magnetic fields. *Phys. Rev.* E **61**, 1890–1898.

LEUNISSEN, M., CHRISTOVA, C., HYNNINEN, A.-P., ROYALL, C., CAMPBELL, A., IMHOF, A., DIJKSTRA, M., ROIJ, R. & VAN BLAADEREN, A. 2005*a* Ionic colloidal crystals of oppositely charged particles. *Nature* **437**, 235–40.

LEUNISSEN, M. E., CHRISTOVA, C. G., HYNNINEN, A.-P., ROYALL, C. P., CAMPBELL, A. I., IMHOF, A., DIJKSTRA, M., VAN ROIJ, R. & VAN BLAADEREN, A. 2005*b* Ionic colloidal crystals of oppositely charged particles. *Nature* **437** (7056), 235–240.

LOWEN, H. 1992 Structure and Brownian dynamics of the two-dimensional Yukawa fluid. *J. Phys.: Condens. Matter* **4** (50), 10105–10116.

LÖWEN, H. 1994 Melting, freezing and colloidal suspensions. *Phys. Rep*. **237** (5), 249–324.

LÖWEN, H. & KRAMPOSTHUBER, G. 1993 Optimal effective pair potential for charged colloids. *Europhys. Lett*. **23** (9), 673–678.

MARRO, J. & DICKMAN, R. 1999 *Nonequilibrium Phase Transitions in Lattice Models*. Cambridge University Press.

MICHEL, F. C. 1991 *Theory of Neutron Star Magnetospheres*. Theoretical Astrophysics, Chicago, London: University of Chicago Press.

NETZ, R. R. 2003 Conduction and diffusion in two-dimensional electrolytes. *Europhys. Lett*. **63** (4), 616–622.

OOHARA, W., DATE, D. & HATAKEYAMA, R. 2005 Electrostatic waves in a paired fullerene-ion plasma. *Phys. Rev. Lett*. **95**, 175003.

OOHARA, W. & HATAKEYAMA, R. 2003*a* Pair-ion plasma generation and fullerene-dimer formation. *Thin Solid Films* **435**, 280–284.

OOHARA, W. & HATAKEYAMA, R. 2003*b* Pair-ion plasma generation using fullerenes. *Phys. Rev. Lett*. **91**, 205005.

OOHARA, W. & HATAKEYAMA, R. 2007 Basic studies of the generation and collective motion of pair-ion plasmas. *Phys. Plasmas* **14** (5), 055704.

OTT, T. & BONITZ, M. 2011 Diffusion in a strongly coupled magnetized plasma. *Phys. Rev. Lett*. **107**, 135003.

PAUL N. ARENDT, J. & EILEK, J. A. 2002 Pair creation in the pulsar magnetosphere. *Astrophys. J*. **581** (1), 451–469.

PILCH, I., PIEL, A., TROTTENBERG, T. & KOEPKE, M. E. 2007 Dynamics of small dust clouds trapped in a magnetized anodic plasma. *Phys. Plasmas* **14** (12), 123704.

PILCH, I., REICHSTEIN, T. & PIEL, A. 2008 Torus-shaped dust clouds trapped in a magnetized anodic plasma. *Phys. Plasmas* **15** (10), 103706.

PIRAN, T. 1999 Gamma-ray bursts and the fireball model. *Phys. Rep*. **314** (6), 575–667.

PIRAN, T. 2005 The physics of gamma-ray bursts. *Rev. Mod. Phys*. **76**, 1143–1210.

REX, M. & LÖWEN, H. 2008 Influence of hydrodynamic interactions on lane formation in oppositely charged driven colloids. *Eur. Phys. J.* E **26**, 143–150.

ROYALL, C. P., LEUNISSEN, M. E., HYNNINEN, A.-P., DIJKSTRA, M. & VAN BLAADEREN, A. 2006 Re-entrant melting and freezing in a model system of charged colloids. *J. Chem. Phys*. **124** (24), 244706.

SAHU, B., PAL, B., PORIA, S. & ROYCHOUDHURY, R. 2015 Nonlinear dynamics of ion acoustic waves in quantum pair-ion plasmas. *J. Plasma Phys*. **81** (5), 905810510.

Sarma, U., Baruah, S. & Ganesh, R. 2020 Lane formation in driven pair-ion plasmas. *Phys. Plasmas* **27**, 012106.

Sato, N., Uchida, G., Kaneko, T., Shimizu, S. & Iizuka, S. 2001 Dynamics of fine particles in magnetized plasmas. *Phys. Plasmas* **8** (5), 1786–1790.

Strümpel, C., Astrov, Y. A. & Purwins, H.-G. 2002 Multioscillatory patterns in a hybrid semiconductor gas-discharge system. *Phys. Rev.* E **65**, 066210.

Sütterlin, K. R., Wysocki, A., Ivlev, A. V., Räth, C., Thomas, H. M., Rubin-Zuzic, M., Goedheer, W. J., Fortov, V. E., Lipaev, A. M., Molotkov, V. I., *et al.* 2009 Dynamics of lane formation in driven binary complex plasmas. *Phys. Rev. Lett*. **102**, 085003.

Tandberg-Hanssen, E. & Emslie, A. G. 1988 *The Physics of Solar Flares*. Cambridge University Press.

Tarama, S., Egelhaaf, S. U. & Löwen, H. 2019 Traveling band formation in feedback-driven colloids. *Phys. Rev.* E **100**, 022609.

Thomas, E., Lynch, B., Konopka, U., Menati, M., Williams, S., Merlino, R. L. & Rosenberg, M. 2019 Pattern formation in strongly magnetized plasmas: observations from the magnetized dusty plasma experiment (MDPX) device. *Plasma Phys. Control. Fusion* **62** (1), 014006.

Uchida, G., Konopka, U. & Morfill, G. 2004 Wave dispersion relation of two-dimensional plasma crystals in a magnetic field. *Phys. Rev. Lett*. **93**, 155002.

Vissers, T., van Blaaderen, A. & Imhof, A. 2011*a* Band formation in mixtures of oppositely charged colloids driven by an ac electric field. *Phys. Rev. Lett*. **106**, 228303.

Vissers, T., Wysocki, A., Rex, M., Löwen, H., Royall, C. P., Imhof, A. & van Blaaderen, A. 2011*b* Lane formation in driven mixtures of oppositely charged colloids. *Soft Matt*. **7**, 2352–2356.

Zank, G. P. & Greaves, R. G. 1995 Linear and nonlinear modes in nonrelativistic electron-positron plasmas. *Phys. Rev.* E **51**, 6079–6090.